Vol3 No1
January 2023
e-ISSN: 2682-9177

AJMed TECH | ASIAN JOURNAL OF MEDICAL TECHNOLOGY

https://doi.org/10.32896/ajmedtech.v3n1

Intracranial hemorrhage detection in ct scan using deep learning
Thermo-pneumatic micropump for drug delivery applications
Smart health monitoring system utilizing internet of things (iot) and arduino
Dose mapping of gamma irradiation chamber (gic)

https://ajmedtech.com

eISSN 2682-9177
9 772682 917006

Editorial Team

ASIAN JOURNAL OF MEDICAL TECHNOLOGY

Contents

Volume 3 **Number 1** **January 2023**

No. *Title* *Page*

balt solutions
for AVM treatment

squid
EVOH co-polymer

sonic
detachable tip microcatheter

balt
inspiring innovation

Join us for Hands-On
AVM Workshops. Register your interest with
carlteh@medcinpharma.com / hiba@medcinpharma.com

MEDCIN PHARMA SDN BHD (587084 - D)

Imported and distributed by :
Medcin Pharma Sdn Bhd (587084-D)
H-G-3A, Blok H, Sekitar 26 Enterprise,
Persiaran Hulu Selangor, Seksyen 26,
40400 Shah Alam, Selangor Darul Ehsan
Tel: +60 (03) 5192 3966
Fax: +60 (03) 5191 9539
http://www.medcinpharma.com

A RANDOMIZED CONTROLLED TRIAL OF JIGSAW VERSUS E-LEARNING APPROACHES: PRACTICAL PARASITOLOGY TRAINING TO IMPROVE PARASITE IDENTIFICATION TECHNIQUES IN CLINICAL LABORATORY SCIENCE EDUCATION

K. Kobayashi[1,2,*], Y. Kosuge[3] and K. Akazawa[1]

[1]Department of Medical Informatics,
Niigata University Medical and Dental Hospital, 951-8510, Niigata, Japan.

[2]Department of Medical Technology,
Kitasato Junior College of Health and Hygienic Sciences, 949-7241, Niigata, Japan.

[3]Department of Medical Technology, School of Nursing and Medical Care,
Yokkaichi Nursing and Medical Care University, 512-8045, Mie, Japan.

[*]Corresponding Author's Email: k-koba@kitasato-u.ac.jp

Article History: Received November 1, 2022; Revised November 23, 2022; Accepted November 24, 2022

ABSTRACT: Japan is witnessing an increase in parasitic diseases caused by contaminated food, international travel, and sexual activity, but much less time is spent on parasitology education. To avoid incorrect identifications, students were required to master the technique in a limited amount of time. This requirement necessitates new and more effective teaching methods that allow students to identify parasites. In this study, we conducted practical parasitology training using two teaching methods. We assigned 33 students to the jigsaw method (class A) and another 33 to the e-learning method (class B). This study aimed to determine the effectiveness and limitations of these teaching methods. Therefore, we conducted an RCT to reduce confounding bias and increase the validity of our results. The primary outcome was the participants' scores in the microscopic test to identify helminth eggs and protozoa in faecal and blood specimens, while the secondary outcome was the participant' scores in the photo test. The results showed that the median scores for the microscopic test were 83.3 for class A and 91.6 for class B ($p = 0.085$), and the mean scores for the photo test were 79.4 for class A and 87.3 for class B ($p = 0.033$). Therefore, the e-learning method was more effective than the

jigsaw method.

KEYWORDS: *Parasitology; Clinical Laboratory Science Education; Jigsaw Method; E-learning*

1.0 INTRODUCTION

In Japan, although public health advancements have lowered the number of soil-transmitted helminth infections, parasitic diseases due to contaminated food, international travel, and sexual activity are increasing [1]. Palmieri et al. highlighted the importance of conducting practical training for accurate diagnoses to address the demand for parasite testing caused by increased globalization [2]. However, Japan has seen a decline in the amount of time spent on parasitology education [3]. Therefore, educational institutions for clinical laboratory technologists require practical training with more effective teaching methods. In parasitology lectures, studies have reported the effectiveness of teaching methods that use flipped learning and problem-based learning [4]. However, no randomized controlled trials have evaluated the effectiveness of teaching methods in practical parasitology training. Therefore, we conducted an RCT to reduce confounding bias and increase the validity of our results. We adopted two teaching methods to conduct the training: the jigsaw method and the e-learning method with a learning management system (Moodle). This study aimed to describe the effectiveness and challenges of these educational methods. The research proposition was that the jigsaw method is better than the e-learning method at improving students' ability to identify parasites. We also predicted that the jigsaw class would attain higher scores than the e-learning class on the microscopic and photo tests. In the jigsaw method, students must assume the role of experts and explain the parasite to others. Therefore, we formulated this hypothesis because we believe students would responsibly participate in the practical training after sufficient preparation.

2.0 METHODOLOGY

2.1 Research Design

2.1.1 Study Design

We conducted a randomized controlled trial to examine how the two teaching methods affect practical parasitology training.

i. Practical training period: January 2017 (follow-up surveys conducted between May 2017 and April 2018)

ii. Practical training hours: 15 (10 sessions of 90 minutes each)

iii. Practical training contents: Observation of helminth egg, larvae, and protozoa (a total of 26 parasite species)

2.1.2 Participants

We recruited 66 students in the first grade of the Department of Clinical Examination at Kitasato Junior College of Health and Hygienic Sciences.

2.1.3 Intervention

i. Jigsaw Method (Class A)

The jigsaw method is a cooperative learning technique in which students interact with and teach one another [5]. According to Colosi et al., the jigsaw method positively affects the teaching of biology experiments with practical training [6]. Therefore, we chose this method because students would responsibly participate in the practical training.

ii. E-learning Method (Class B)

We uploaded videos, photos, and quizzes to Moodle, an open-source learning platform. Abdul suggested that traditional parasitology education would benefit from a Web-based teaching system as a support tool [7]. With e-learning, students can undergo virtual practical training as often as they wish, with no time or location constraints. Therefore, we selected this method because conducting practical training virtually in advance will facilitate real-world practical training.

2.1.4 Outcome Measures

The primary outcome was students' scores on the microscopic test. The

microscopic test contained three questions per category (i.e., nematodes, trematodes, cestodes, and protozoa) for 12 questions. Meanwhile, the secondary endpoint was students' scores on the photo test. The photo test involved photographic identification, with five questions per category (i.e., nematodes, trematodes, cestodes, and protozoa) for 20 questions. Percentages of correct answers were calculated. Exploratory outcomes were the longitudinal changes in students' photo test scores and questionnaire results.

2.1.5 Sample Size

Before this study, parasitology lectures were conducted using two teaching methods: active learning and e-learning [8]. Based on these results, the class scores were 15 points higher for the jigsaw method than for the e-learning method. The sample size was estimated with a standard deviation of 22 points for each class score, a significance level (alpha) of 0.05, and a power of 0.8. This resulted in 35 participants per class when following a 1:1 assignment. Since the study involved 33 participants per group, its power was 0.78.

2.1.6 Randomization

Random assignment was conducted using minimization, using three factors to adjust for allocation: gender, age (<20 years or ≥20 years; the age of majority or not the age of majority), and parasite photograph pretest results (scored or not scored). We used the minimization method to produce the random assignment for two reasons: the small sample size of the classes and the need to reduce differences among prognostic factors.

2.1.7 Blinding

This manuscript was based on an open-label study.

2.1.8 Ethical Considerations

All participants attended a briefing session and provided consent forms. Approval was obtained from the Ethics Committee of Niigata University and Kitasato Junior College of Health and Hygienic Sciences.

2.2 Teaching Methods

2.2.1 Jigsaw Method (Class A)

The teacher assigned one species of parasite eggs to each of the six teams (groups A–F), which were designated as expert groups for that species (Figure 1). Each team consisted of five to six students. The participants shared information with their expert team members for 20 minutes while examining their assigned eggs under a microscope (expert activity).

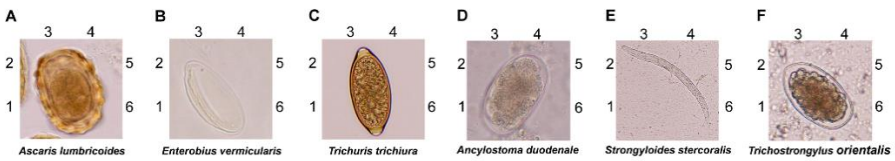

Figure 1: Expert teams: letters indicate groups; numbers indicate members

New round groups comprised one member selected from each expert team (Figure 2). The expert had five minutes to describe the eggs to the other students. Afterwards, the students observed and recorded the results on their worksheets for 20 minutes. The round groups then moved to the next table by turns. The teacher facilitated the activity to ensure that the practical training was conducted smoothly.

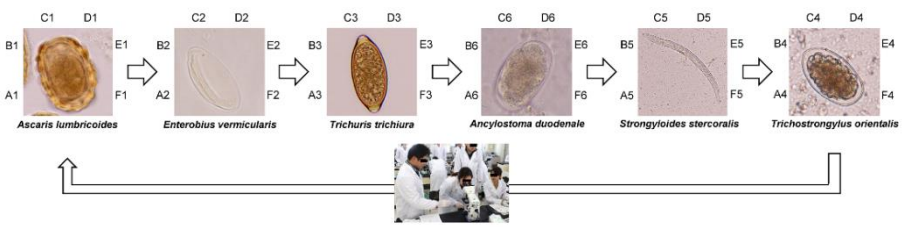

Figure 2: New round groups: alphanumeric codes represent team members from the expert team

2.2.2 E-learning Method (Class B)

The participants viewed an egg detection video and identification slide using Moodle and then answered egg photo quizzes before undergoing practical training. The students spent 25 minutes observing and recording each specimen during the training. The teacher provided direct instructions to participants who had difficulty detecting the eggs.

i. Egg detection video (Figure 3)

Videos of the egg detection process were recorded under a microscope at 4×, 10×, and 40× magnification. A video was 1.5 minutes on average, and 29 movies were recorded.

Figure 3: Egg detection video (example: unfertilized egg of *Ascaris lumbricoides*)

ii. Egg identification slide (Figure 4)

This educational material allows the user to reproduce changes similar to when a microscope's focus is fine-tuned using a fine-adjustment screw by clicking on the slide. A total of 23 specimens were used.

Figure 4: Egg identification slide (example: egg of *Hymenolepis nana*); clicking the image changes the view from ① to ② to ③ to ④

iii. Egg photo quiz (Figure 5)

After viewing the egg detection videos and identification slides, the participants answered several egg picture quizzes containing 30 questions.

Figure 5: Egg photo quiz (example: egg of *Schistosoma mansoni*)

2.3 Statistical Analysis

We used a box-and-whisker plot to represent the score distribution for the microscopic test. We performed the Wilcoxon rank-sum test to compare the scores of the two groups and expressed the difference as a Hodges–Lehmann estimator (HLE) and 95% confidence intervals. We estimated the sample size using a t-test but adopted a nonparametric method because the actual score distribution was skewed. We also used Fisher's exact test to compare the baseline characteristics and compare the percentages of correct responses for each microscopic test. We performed Welch's t-test to compare the photo test scores. We assessed longitudinal changes in photo test scores using a linear mixed-effects model for repeated measures (MMRM) in which the objective variable was the photo test score, and the explanatory variables were time, class, and their interactions. This model assumed an unstructured covariance error structure, and degrees of freedom were adjusted using Satterthwaite's method. We performed the Wilcoxon rank-sum test for interclass comparisons of questionnaire response rates and the Bowker test for intraclass comparisons. Test results were considered statistically significant at $p < 0.05$. For statistical analyses, we used SAS 9.4 and JMP PRO 16.2 (SAS Institute Inc., Cary, NC, USA).

3.0 Results

3.1 Overview of the Randomized Controlled Trial (Figure 6)

We observed no significant differences in the allocation factors at baseline (Table 1). All students completed the practical training with perfect attendance.

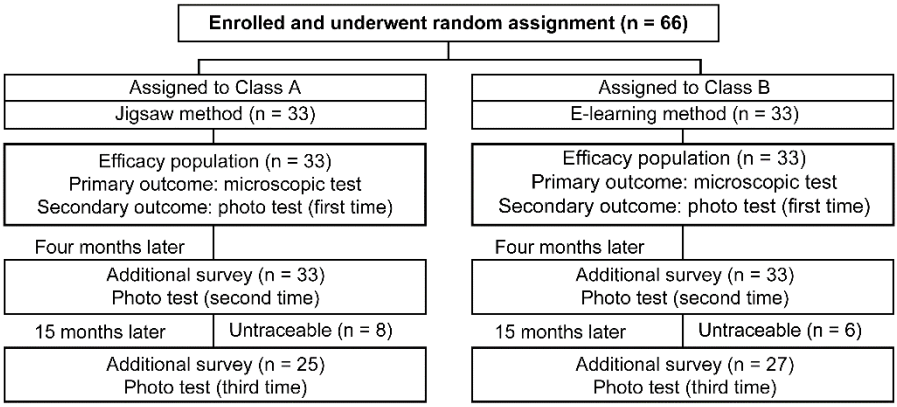

Figure 6: Trial profile

Table 1: Baseline demographics and characteristics of the intention to treat population

Characteristics	Class A (n = 33)	Class B (n = 33)	Total (n = 66)	p-value
Gender				
Male	12 (36.4%)	13 (39.4%)	25 (37.9%)	0.99
Female	21 (63.6%)	20 (60.6%)	41 (62.1%)	
Age				
20 years old and over	6 (18.2%)	5 (15.2%)	11 (16.7%)	0.99
Under 20 years old	27 (81.8%)	28 (84.8%)	55 (83.3%)	
Pretest score				
Scored	16 (48.5%)	14 (42.4%)	30 (45.5%)	0.81
Not scored	17 (51.5%)	19 (57.6%)	36 (54.4%)	

3.2 Primary Outcome (Microscopic Test)

Figure 7 shows the score distribution for the microscopic test. While the HLE was 8.3 points higher for class B than for class A, this difference was not statistically significant (Figure 7). Four parasites differed in the percentage of correct responses by more than 10 points, which were all higher in class B than in class A (Table 2).

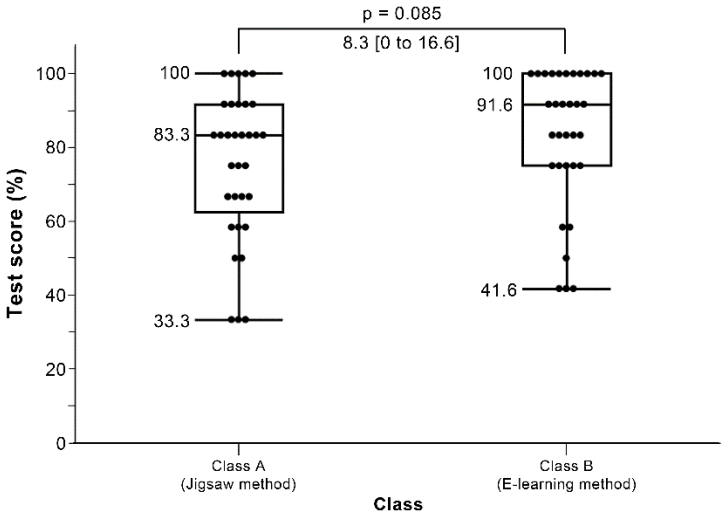

Figure 7: Microscopic test scores per class

Table 2: Percentage of correct responses by question and differences between class A and class B

Genus	No.	Species	Class A	Class B	Difference [95%CI]	p-value
Nematoda	1	*Ascaris lumbricoides*	93.9	100	6.1 [−5.1 to 17.2]	0.49
	2	*Ancylostoma duodenale*	75.8	69.7	−6.1 [−30.4 to 18.4]	0.78
	3	*Trichuris trichiura*	97.0	93.9	−3.1 [−16.1 to 10.0]	1
Trematoda	4	*Clonorchis sinensis*	51.5	69.7	18.2 [−8.0 to 44.4]	0.21
	5	*Metagonimus yokogawai*	57.6	72.7	15.1 [−10.6 to 40.9]	0.30
	6	*Schistosoma mansoni*	81.8	84.8	3.0 [−18.0 to 24.0]	1
Cestoda	7	*Diphyllobothrium nihonkaiense*	54.5	81.8	27.3 [2.8 to 51.8]	0.032
	8	*Hymenolepis diminuta*	66.7	78.8	12.1 [−12.2 to 36.4]	0.41
	9	*Taenia saginata*	87.9	90.9	3.0 [−14.8 to 20.9]	1
Protozoa	10	*Balantidium coli*	84.8	90.9	6.1 [−12.7 to 24.8]	0.71
	11	*Plasmodium vivax*	54.5	63.6	9.1 [−17.6 to 35.7]	0.62
	12	*Trichomonas vaginalis*	100	97.0	−3.0 [−11.9 to 5.9]	1

3.3 Secondary Outcome (Photo Test)

The mean score was 7.9 points higher for class B than for class A—a significant difference. The variance of scores for class B was significantly smaller than that for class A (F-statistics = 0.41, p = 0.015), with 60 being the lowest score (Table 3).

Table 3: Comparison of photo test scores between classes A and B

Class	n	Mean	Median	Max	Min	SD	Mean difference between Class B and Class A [95%CI]	p-value
A	33	79.4	80	100	35	17.4	7.9 [0.7 to 15.1]	0.033
B	33	87.3	90	100	60	11.2		

3.4 Exploratory Outcomes

3.4.1 Longitudinal Changes in Photo Test Scores

Figure 8 presents changes in scores up to 15 months. The results of the MMRM analysis showed that the time–class interaction was not statistically significant (p = 0.764). Thus, the mean scores for both teaching methods varied similarly over time, but those for class B were always higher than those of class A.

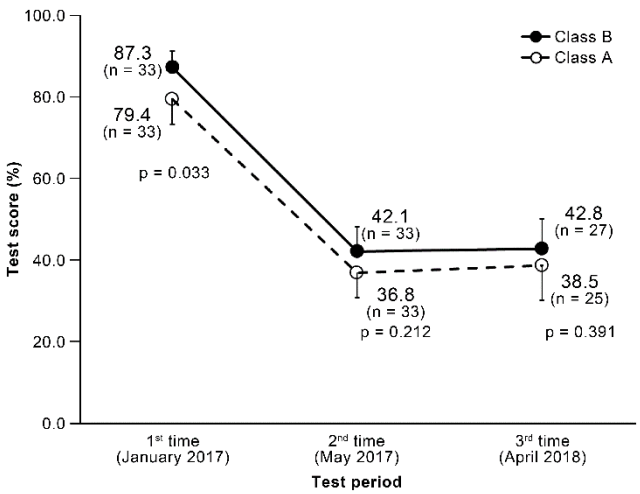

Figure 8: Mean scores up to 15 months later; error bars indicate a 95% confidence interval for the mean

3.4.2 Questionnaire Results

Table 4 shows the questionnaire table**.** The response rate was 100%. No items indicated significant differences between classes; however, class B tended to show higher self-efficacy in identifying parasites than class A (no. 3). In the jigsaw activity, students in class A were able to share information but were unable to explain it to others. Students in class B had a slight tendency not to use Moodle for review.

Table 4: Results of the questionnaire on practical training; data are represented as the number of students (proportion)

Item	No.	Question	Class	Response[i]					p-value[ii]
				①	②	③	④	⑤	
Self-assessment	1	Did you actively conduct your preparatory studies?	A	22 (66.7)	7 (21.2)	3 (9.1)	1 (3.0)	0 (0)	0.915
			B	21 (63.6)	9 (27.3)	3 (9.1)	0 (0)	0 (0)	
	2	Were you willing to do the practical training?	A	27 (81.8)	6 (18.2)	0 (0)	0 (0)	0 (0)	0.556
			B	25 (75.8)	8 (24.2)	0 (0)	0 (0)	0 (0)	
	3	Do you think you have mastered the ability to identify parasite using a microscope?	A	19 (57.6)	12 (36.4)	2 (6.0)	0 (0)	0 (0)	0.098
			B	25 (75.8)	8 (24.2)	0 (0)	0 (0)	0 (0)	
Satisfaction	4	Was the training satisfactory overall?	A	25 (75.8)	8 (24.2)	0 (0)	0 (0)	0 (0)	0.239
			B	29 (87.9)	3 (9.1)	1 (3.0)	0 (0)	0 (0)	
Jigsaw activities	5	Did you share information in advance within your team of experts?	A	23 (69.7)	7 (21.2)	2 (6.1)	1 (3.0)	0 (0)	0.018
	6	Were you able to explain yourself well to others as an expert?		9 (27.3)	16 (48.5)	7 (21.2)	1 (3.0)	0 (0)	
Using Moodle[iii]	7	Did you use Moodle to do your preparatory studies before each practical training?	B	25 (75.8)	5 (15.2)	2 (6.0)	1 (3.0)	0 (0)	0.416
	8	Did you use Moodle for your review?		17 (51.5)	8 (24.2)	4 (12.1)	1 (3.0)	3 (9.1)	

i) Responses: ① agree, ② slightly agree, ③ neither, ④ slightly disagree, and ⑤ disagree. ii) Nos. 1–4: Wilcoxon rank-sum test; a combination of nos. 5 and 6 and nos. 7 and 8: Bowker test. iii) All students in class B entered Moodle based on its access logs. Among the students, 19 (57.6%) used all the materials, and 26 (79%) used more than 80%.

4.0 DISCUSSION

We conducted this study to verify the effectiveness of teaching methods in practical parasitology training. Although not significantly different, class B had a higher median score than class A. Specifically, class B also tended to attain higher scores in the parasites Trematoda and Cestoda, which are essential to be distinguished from other similarly shaped eggs (e.g., *Clonorchis sinensis* and *Metagonimus yokogawai*). We considered the eggs to be well-identified by class B. Class B scored significantly higher on the photo test than class A,

scoring 60 or higher. For both classes, we halved the scores on the second photo test. These results were consistent with those of Shomaker et al., who reported that scores on a photo test after a lecture were reduced by half after four months [9]. Both teaching methods showed similar longitudinal changes, but class B tended to attain consistently higher mean scores than class A. This observation shows that the e-learning method may be more effective for knowledge retention. Contrary to our hypothesis, the scores for the e-learning method were higher than those for the jigsaw method. The reasons are as follows.

The jigsaw method promotes student-centred and motivated practical training [6], but its effectiveness depends on the appropriate teaching materials, students' willingness to participate, and information accuracy [6,10,11]. In this study, students did not present incorrect information because the teacher had checked the prepared content in advance. Based on the questionnaire results, 81.8% of class A reported being actively engaged in practical training. Although 69.7% of the students shared information with a professional team, only 27.3% could explain the content to others. The open-ended comments in the questionnaire highlighted that some students needed detailed explanations from the teacher. Mori reported that, in active learning, a certain number of students felt anxious about not understanding the content because of the low quality of internalization [12]. Therefore, we presume that teachers must assist with internalization. As a countermeasure, conducting a preassessment test, such as the iRAT and tRAT in team-based learning, was necessary [13].

The e-learning method is characterized by flipped learning [14], in which students use the knowledge they acquired from virtual practical training in real practical training. Studies have verified the effectiveness of flipped learning in Asian universities [15].

The Moodle access logs showed that about 80% of the students used more than 80% of the course materials. Therefore, we considered that the e-learning program was successful. The questionnaire results indicated that students in class B who acquired identification skills scored 18.2 points higher than those in class A; hence, class B had more students who felt a sense of self-efficacy. Satisfaction with practical training was also increased. We hypothesized that virtual practical training would lead to real practical training, which would not only improve test scores but would also produce psychological advantages. Besides the benefits of the virtual practical training provided by

Moodle materials, another beneficial aspect was involved: the teacher's individual instructions' effect on students who could not identify parasites. Students who already had a sufficient understanding of the content from the virtual practical training could conduct practical training without direct instructions from the teacher. Therefore, the teacher could take their time in providing individual instructions to students with identification challenges.

Based on these results, we conclude that the e-learning method is more effective in improving performance than the jigsaw method. This study was an RCT adjusted for three possible confounding factors. Although the sample size was insignificant, the confounding bias for the results obtained was suppressed as far as possible. Therefore, we expected that the validity of the results would be ensured.

In medical education, e-learning is a valuable method that complements traditional lectures [16]. Digital images, videos, and virtual microscopes are necessary Web-based educational materials for parasitology education [4,7,17–19]. Educational materials that incorporate gamification elements are also helpful [20]. In the future, we aim to improve the e-learning materials created in this study and use them to deliver not only education at the technical college but also practical education.

This study has several limitations. We did not assess attitudes toward the jigsaw method. If each student had been regularly provided feedback on the evaluation results, their scores could have improved. However, it took much work for one teacher to evaluate all 33 students. In the e-learning method, we did not enforce the use of Moodle materials because of the upper limit of the communication volume of personal devices. Therefore, not all students used all the materials, but we infer that their scores would have been even higher had they all done so. Donkin et al. showed that not only did students engage with the e-learning materials before participating in the training, but teachers also provided feedback after the training was complete, significantly improving student performance [21]. In the future, we must improve our teaching methods to allow space for feedback to be given to the students.

5.0 CONCLUSIONS

This study sought to verify the effectiveness of jigsaw and e-learning methods in practical parasitology training. Based on the student's performance in the microscopic and photo tests, we found that the e-learning method was more effective than the jigsaw method. Enhancing e-learning materials and improving the utilization rate of LMS is essential for students to learn techniques within a limited period.

6.0 ACKNOWLEDGMENTS

We thank the 66 individuals who participated in this study. The authors thank Enago (www.enago.jp) for the English language review.

7.0 REFERENCES

[1] Y. Sato, "Recent State of Parasitoses in Japan—Epidemiology for clinicians", *Japan Medical Association Journal*, vol. 48, no. 3, pp. 148-154, 2005.

[2] J.R. Palmieri, S.F. Elswaifi and K.K. Fried, "Emerging need for parasitology education: training to identify and diagnose parasitic infections", *The American Society of Tropical Medicine and Hygiene*, vol. 84, no. 6, pp. 845-846, 2011. https://doi.org/10.4269/ajtmh.2011.10-0733

[3] S. Sekine, "Pre-graduate teaching of human parasitology for medical laboratory technologist programs in Japan", *Humanities and Social Sciences Communications*, vol. 9, no. 225, pp.1-6,2022. https://doi.org/10.1057/ s415 99-022-01246-w

[4] A. Jabbar, R.B. Gasser and J. Lodge, "Can new digital technologies support parasitology teaching and learning?", *Trends in Parasitology*, vol. 32, no. 7, pp. 522-530, 2016. https://doi.org/10.1016/j.pt.2016.04.004

[5] E. Aronson. (2002). *Chapter 10 - Building Empathy, Compassion, and Achievement in the Jigsaw Classroom* [Online]. Available: http://cachescan.bcub.ro/e-book/E2/580695/209-278.pdf

[6] J.C. Colosi and C.R. Zales, "Jigsaw cooperative learning improves biology lab courses", *BioScience*, vol. 48, no. 2, pp. 118-124, 1998. https://doi.org/10.2307/1313137

[7] R. Abdul-Ghani, "Towards e-parasitology: making use of virtual microscopy", *Tropical Medicine & International Health*, vol. 20, no. 2, pp. 227-229, 2015. https://doi.org/10.1111/tmi.12426

[8] K. Kobayashi, "Evaluation of teaching methods in parasitology lectures: a randomized crossover trial of active learning and e-learning methods" [in

Japanese], *Japanese Journal of Medical Technology Education*, vol. 11, no. 2, pp. 165-174, 2019.

[9] T.S. Shomaker, D.J. Ricks and D.C. Hale, "A prospective, randomized controlled study of computer-assisted learning in parasitology", *Academic Medicine*, vol. 77, no. 5, pp. 446-449, 2002. https://doi.org/10.1097/00001888-200205000-00022

[10] M.J. Bose, P.C. Jarreau, L.W. Lawrence and P. Snyder, "Using cooperative learning in clinical laboratory science education", *Clinical Laboratory Science*, vol. 17, no. 1, pp. 12-18, 2004.

[11] K. Soundariya, M. Senthilvelou, S.S. Teli, V. Deepika, K.S. Selvi and S.M. Mangalavalli, "Jigsaw technique as an active learning strategy in Physiology for I MBBS Students", *Biomedicine*, vol. 41, no. 3, pp. 654-659, 2021. https://doi.org/10.51248/.v41i3.291

[12] T. Mori. (2018). "*The Flipped Classroom: An Instructional Framework for Promotion of Active Learning*", In: K. Matsushita (ed.), Deep Active Learning [Online]. Available: https://doi.org/10.1007/978-981-10-5660-4_6

[13] M. Nyindo, J. Kitau, E. Lisasi, G. Kapanda, J. Matowo, P. Francis and J. Bartlett. "Introduction of team-based learning (TBL) at Kilimanjaro Christian Medical University College: experience with the ectoparasites module", *Medical Teacher*, vol. 36, no. 4, pp. 308-313, 2014. https://doi.org/10.3109/0142159X.2013.876490

[14] J. Bergmann and A. Sams. (2012). *Flip Your Classroom, Reach Every Student in Every Class Every Day* [Online]. Available: https://www.rcboe.org/cms/lib/ga01903614/centricity/domain/15451/flip_your_classroom.pdf

[15] C.S.M. Joanne and F. Lateef, "The flipped classroom: viewpoints in Asian universities", *Education in Medical Journal*, vol. 6, no. 4, pp. 20-26, 2014.

[16] J.G. Ruiz, M.J. Mintzer and R.M. Leipzig, "The impact of e-learning in medical education", *Academic Medicine*, vol. 81, no. 3, pp. 207-212, 2006. https://doi.org/10.1097/00001888-200603000-00002

[17] E. Linder, M. Lundin, C. Thors, M. Lebbad, J. W-Krusnell, H. Helin, B. Leiva, J. Isola and J. Lundin, "Web-based virtual microscopy for parasitology: a novel tool for education and quality assurance", *PLOS Neglected Tropical Diseases*, vol. 2, no. 10, pp. 1-8, 2008. https://doi.org/10.1371/journal.pntd.0000315

[18] A. Peña-Fernández, L. Acosta, S. Fenoy, A. Magnet, F. Izquierdo, F.J. Bornay, M.D. Ollero, C. Hurtado and C.D. Aguila, "Evaluation of a novel digital environment for learning medical parasitology", *Higher Education Pedagogies*, vol. 5, no. 1, pp. 1-18, 2020.

[19] L. Ahmed, L. H .Seal, C. Ainley, B. De la Salle, M. Brereton, K. Hyde, J. Burthem and W.S. Gilmore. "Web-based virtual microscopy of digitized blood slides for malaria diagnosis: an effective tool for skills assessment in different countries and environments", *Journal of Medical Internet Research*, vol. 18, no. 8, p. e213, 2016. https://doi.org/10.2196/jmir.6027

[20] A. Peña-Fernández, L. Acosta, T. Sgamma, M.D. Evans and J. Sampson-Brindley, "Educational e-Parasitology games built in an app for smartphones: development and framework", in EduLearn2021, Palma de Mallorca, 2021, pp. 7867-7872. https://doi.org/10.1080/23752696.2019.1710549

[21] R. Donkin, E. Askew, and H. Stevenson, "Video feedback and e-Learning enhances laboratory skills and engagement in medical laboratory science students", *BMC Medical Education*, vol.19, no.310, 2019. https://doi.org/10.1186/s12909-019-1745-1

BLOOD MIMICKING FLUID FOR APPLICATION IN ANGIOGRAPHY IMAGING: THE EFFECT OF SURFACTANT ADDITION TOWARDS DENSITY AND VISCOSITY

S.J. Chai[1,*], A.S. Shuib[1], S.W. Phang[1], A.S. Muda[2,3] and M.I. Ahmad Sabri[3]

[1]School of Engineering, Faculty of Innovation and Technology, Taylor's University, 47500 Subang Jaya, Selangor, Malaysia.
[2]Radiology Department, Hospital Pengajar University Putra Malaysia, 43400 , Serdang, Selangor, Malaysia.
[3]Lönge Medikal Sdn Bhd, Putra Science Park, 43400 , Serdang, Selangor, Malaysia.

[*]Corresponding Author's Email: chaishanjet@sd.taylors.edu.my

Article History: Received January 5, 2023; Revised January 25, 2023; Accepted anuary 25, 2023

ABSTRACT: Modern 3D anatomical modelling and surgical simulation provide surgeons with technical training to practice realistic pre-surgery rehearsals, adapt to patient-specific anatomical structures and prepare for operation procedures with minimal health risks to patients. Blood-mimicking fluid is a biomimetic innovation developed for 3D medical simulator applications to mimic the non-Newtonian fluid properties of human blood. The ongoing challenge in blood mimicking fluid development is to replicate the shear-thinning behaviour and apparent viscosity of blood over a shear rate range of 0-1000 s^{-1} that occurs in human blood vessels. There is a limited investigation about the effect of surfactant concentration towards the density and viscosity of a blood-mimicking fluid. Surfactant is added in blood mimic to ensure the mixing of materials is homogenous. This research investigates the effect of surfactant addition in blood-mimicking fluids comprised of water-glycerol-based fluid, xanthan gum, corn starch and contrast agent. The density and viscosity were analyzed using a rheometer and densitometer, respectively. The increase of surfactant concentration in the blood-mimicking fluid is discovered to have no significant influence on the blood-mimicking fluid density but increased the overall shear-thinning viscosity of the blood-mimicking fluid.

***KEYWORDS**: Blood Mimicking Fluid; Blood Analogue Fluid; Surfactant;*

Viscosity; Density.

1.0 INTRODUCTION

Medical surgical simulation is continuously researched to develop cutting edge, state-of-the-art equipment that are expanding the medical and biomedical engineering sector. Surgical simulator is one such pivotal tool that is being designed to advance the realism of pre-surgery operations as training and rehearsal for surgeons of novice or experienced backgrounds to acquire the proper surgical skills, self-awareness, and self-confidence, without jeopardizing the health safety and success rate of live patients in the actual surgery. Traditional surgical simulation includes the application of animal subjects, cadavers, and standard human mannequin to provide simplified human anatomies without presenting specific physiological and pathological rare conditions, which can result with lack of understanding and response measure on unique anatomical complications during clinical practice.

With present innovation, modern three-dimensional (3D) blood anastomosis modelling and surgical simulation utilizes 3D printing technology capable of manufacturing extremely complicated geometries, to accurately reproduce a realistic replica of patient-specific anatomical structures. The 3D anatomical replicas are accessible for surgeons to gain technical proficiency in adapting the pathological conditions, applying appropriate operating gestures, and planning successful procedures with minimal operative risks [1].

It becomes clear that with these 3D printed anatomical replica simulations gaining preferences of surgeons and popularity in the medical industry, the biomimetic materials applied in the specified application also need developments for accurate and realistic characteristics that assist surgeons on tactile and visual feedbacks of blood and tissue deformation [2]. One such material innovation is the blood mimicking fluid or blood analogue fluid as another term, which is developed to replicate the physical, chemical, rheological and acoustical properties of real human blood for application in surgical simulations.

Over the past decades, a number of blood mimicking fluid formulations have been proposed in regards of the development of Doppler ultrasound and magnetic resonance (MR) angiography imaging performance, which non-invasively assess crucial blood

parameters while ensuring the patient's health safety and comfort [3]. Correspondingly, the sanitary and technical difficulties in handling biological blood by medical personnel during vitro experiment and medical simulation are reduced with the introduction of blood mimicking fluid solution.

Generally, a blood mimicking fluid formulation comprises of the primary water-glycerol base fluid that mimics a blood plasma, followed by adding other constituent materials that are suspended in the base fluid and manipulates the overall properties and characteristics of the blood mimicking fluid. The ongoing challenge in developing blood mimicking fluid formulations is the degree of similarity that the blood mimicking fluid can replicate a human blood, especially the non-Newtonian rheological characteristics of blood.

According to International Electrochemical Commission (IEC) 1685 specifications, the specified viscosity to achieve for a blood mimicking fluid must be approximately 4.0±0.4 mPa.s to resemble the asymptotic of blood that ranges from 3.5-5.55 mPa.s, while the overall blood mimicking fluid density is specified as 1.050±0.040 kg/m^3 which is closely identical the density of water, so that blood mimic component particles of identical density can remain buoyantly suspended in the base fluid [4].

In terms of fluid flow rheology, shear-thinning fluids reflects to the effect of shear stress deformation, as the apparent viscosity of the fluid decreases when subjected to increasing shear rates on a logarithmic scale. The power law equation computed in Equation 1 describes the relation of the apparent viscosity relative to shear rate [5].

$$\mu = k\dot{\gamma}^{n-1} \quad (1)$$

where, μ is the apparent viscosity, $\dot{\gamma}$ is the shear rate, k signifies the fluid consistency index and n represents the non-Newtonian fluid behaviour index.

Presently, there are limited studies conducted on the effect of different surfactant concentration towards the viscosity and density of blood mimicking fluid during blood mimicking fluid formulation for angiography application. Most of the application focused on ultrasound measurement [6]. From a previous study conducted by Goncalves et al. on surfactant's role in blood mimicking fluid, the study is developing a multiphase blood mimicking fluid with the application

of Brij L4 surfactant suspended in pure water, with concentrations of 0.5 to 10 wt% of surfactant evaluated [7].

Another past research study conducted by Oglat et al. is referred for the blood mimicking fluid mixture proposed, comprising of distilled water, propylene glycol and glycerol [8]. For the purpose of dispersing the scattering particles used in blood mimicking fluid, a non-ionic surfactant was added in different amount in order to investigate the important properties influenced by the different surfactant compositions. For the viscosity of the proposed blood mimicking fluid however, Oglat et al. reported findings that supports the work of Goncalves et al. that an increasing viscosity from 0 mPa.s to 35 mPa.s was observed with the linearly increasing non-ionic surfactant concentrations of 1-7 wt% added [8].

The primary objectives of this research are to analyze the effect of surfactant on viscosity and density of blood mimicking fluid compositions through quantitative tests analysis, and to compare the viscosity and density experimental results with biological blood. Contrast agent is considered in the formulation for application in angiography imaging technique.

2.0 METHODOLOGY

2.1 Materials

The blood mimicking fluid sample formulation comprises of distilled water, 99.5% purity of glycerol (Sigma Aldrich, US), xanthan gum from Xanthomonas campestris (Sigma Aldrich, US), corn starch (Sigma Aldrich, US), Omnipaque Iohexol contrast agent (GE Healthcare Shanghai, China) and Synperonic A7 alcohol ethoxylate surfactant (Croda Pte Ltd, Singapore).

2.2 Preparation of Blood Mimicking Fluid

The base fluid mixture that functions as a suspension medium for other blood mimicking fluid components and a control reference sample, was prepared with a weight composition of 60 wt% distilled water and 40 wt% glycerol. The higher constituent ratio of glycerol added was set to achieve a higher overall viscosity level of the specified mixture since glycerol is more viscous, in order to have the base fluid attain an equivalence of the average haematocrit level for human at 40.1%. Blood mimicking fluid samples categorized into five sample sets of

varying weight compositions of distilled water, xanthan gum (XG), corn starch (CS), and Synperonic A7 surfactant (SA), while the weight composition of glycerol and volume of contrast agent added were kept constant. Depending on the blood mimicking fluid sample's composition, the individual components were calculated for their amount to be added according to the weight percentage composition set for the sample and their corresponding weight. Following that, the required amount for a particular material was measured using an analytical balance. For blood mimicking fluid components that are handled in terms of volume, they were measured and prepared using a measuring cylinder. Once the individual component materials were prepared at the right quantity, they are mixed all together using a hot plate magnetic stirrer.

i. Preparation of Base Fluid

The water-glycerol base fluid is prepared by mixing distilled water and glycerol, under constant stirring by the hot plate magnetic stirrer. Firstly, the weights of glycerol and water corresponding to sample's weight percentage composition were calculated to produce a 250 ml worth of sample.

After calculating out the correct weights, the amount for both components were measured and prepared using measuring cylinders, followed by gradually pouring glycerol into the water containing in a beaker while subjected to a constant stirring rate of 400 rpm, at 25 °C. Once the two components have mixed homogenously and formed a clear, transparent solution after 10 minutes, the base fluid is transferred into labelled plastic storage bottles and store in a chemical chiller at 5 °C, to cease microbial activities and prevent biodegradation for long-term storage. The composition of the base fluid sample comprised of 60 wt% of water and 40 wt% of glycerol (Set A).

ii. Addition of Surfactant and Polysaccharides

Table 1 tabulates the compositions of blood mimicking fluid samples from Set B, C and D, with each sample set assigned with a different experimental objective to investigate but in general, the objectives are mainly related to investigating the effect of surfactant concentration added. Set B comprises of blood mimicking fluid samples that contains the water-glycerol base fluid, increasingly added with surfactant. After preparing the base fluid, the specific amount of surfactant was gradually added into it from a small beaker and magnetically stirred

for 20 minutes at 25 °C until the mixture turned opalescent, ready to be transferred into storage bottles and stored in the chemical chiller at 5°C.

Table 1: Blood mimicking fluid samples composition

Experimental Objective	Samples	Components	Composition Ratio (wt/wt%)				
			Water	Glycerol	XG	CS	Surfactant (SA)
Effect of surfactant amount added on blood mimicking fluid base fluid	B1	Water: Glycerol: SA	59.50	40.00	-	-	0.50
	B2		59.10	40.00	-	-	0.90
	B3		58.50	40.00	-	-	1.50
	B4		58.00	40.00	-	-	2.00
Effect of surfactant amount added on blood mimicking fluid composition containing XG	C1	Water: Glycerol: XG:SA	59.99	40.00	0.01	-	-
	C2		59.49	40.00	0.01	-	0.50
	C3		59.09	40.00	0.01	-	0.90
	C4		58.49	40.00	0.01	-	1.50
	C5		57.99	40.00	0.01	-	2.00
Effect of surfactant amount added on blood mimicking fluid composition containing XG and CS	D1	Water: Glycerol: XG:CS:SA	59.98	40.00	0.01	0.01	-
	D2		59.48	40.00	0.01	0.01	0.50
	D3		59.08	40.00	0.01	0.01	0.90
	D4		58.48	40.00	0.01	0.01	1.50
	D5		57.98	40.00	0.01	0.01	2.00

For Set C and D, polysaccharides (XG and CS) are added with a fixed amount of 0.01 wt% respectively into blood mimicking fluid sample compositions, with varying surfactant concentration added. The specified weightage amount of XG and CS added is according to the peer recommendation of a previous research that discovered blood mimicking fluid with 0.01 wt% of XG and CS each suspended in the base fluid exhibits viscosity with the highest similarity to human blood, among other blood mimicking fluid formulations [9].

After the base fluid was prepared, the specific amount of XG and CS were weighted using an analytical balance to measure as the amount

of XG and CS added. With the correct quantities for both XG and CS carefully prepared, they are transferred into the base fluid starting with XG, followed by CS while the mixture is constantly stirred using the hot plate magnetic stirrer for homogeneity in the mixture solution.

Since the polysaccharides are harder to disperse in the base fluid and capable of clumping together easily, the solution was to constantly stir the sample mixture at a higher stirring rate of 600 rpm, at 55 °C for an average of 30 minutes each sample until the lumps were absent and fully dispersed. Following that, the appropriate amount of surfactant is gradually transferred into the sample mixture under the same constant stirring settings. Once the sample mixtures turned opalescent, the samples are immediately transferred into storage bottles and stored in the chiller at 5 °C, to inhibit any microbial growth that can cause biodegradation of the blood mimicking fluid samples.

iii. Addition of Contrast Agent

For the last samples of set E, Table 2 tabulates the formulated sample compositions which include the addition of contrast agent with XG, CS and varying amount of surfactant added into the blood mimicking fluid samples.

Table 2: Blood mimicking fluid samples composition with contrast agent (CA)

Experimental Objective	Samples	Components	Composition Ratio (wt/wt%)				
			Water	Glycerol	XG	CS	SA
Effect of surfactant amount added on blood mimicking fluid composition containing XG, CS and CA	E1	Water: Glycerol: XG:CS: SA CA (constant of 4 v/v %)	59.98	40.00	0.01	0.01	-
	E2		59.48	40.00	0.01	0.01	0.50
	E3		59.08	40.00	0.01	0.01	0.90
	E4		58.48	40.00	0.01	0.01	1.50
	E5		57.98	40.00	0.01	0.01	2.00

Similar to the sample preparation procedure for samples that contain polysaccharides, an extension step is to add a fixed volume of CA into the mixture containing the polysaccharides dissolved in base fluid, followed by adding surfactant as the last component. According to the angiocardiographic procedures recommended for Omnipaque 350 CA, the recommended dosage added for adult patients is 3 ml to 14 ml for arteriography procedure, with 10 mL dosage as the usual CA volume

injected into bloodstreams for adult angiography [10]. Therefore, a fixed volume of 10 mL CA which corresponds to 4 v/v %was added into each sample of Set E via a 10 ml syringe, followed by magnetically stirring the new mixture at 600 rpm for another 20 minutes. Following that, surfactant is then gradually added into the sample mixture and continue with the same constant stirring conditions until the sample mixture turn homogenous and opalescent in appearance. Once the sample was mixed thoroughly, it was stored in the chiller at 5°C.

iv. Density Measurement

The Anton Par DMA 35 Basic handheld digital density meter was utilized to measure the density of all the different blood mimicking fluid samples prepared for this experiment. The density meter is used to directly collect the blood mimicking fluid samples with the help of its in-built pump and subsequently measure their density value on spot, with an uncertainty of ±0.001 g/cm3 and ±0.2 °C for density and temperature respectively. After pumping in the specimen of the samples, the integrated hydrometer processes the specimen's density and specific gravity at certain temperature, displaying the validated final result within a minute interval.

The results are digitally displayed with the final density or concentration at a final temperature reading taken for quantitative analysis, and only 2 mL of sample specimen is required to give the result without wasting unnecessary quantity of sample. Prior to collecting samples with the density meter, the filling tube of the specified equipment needs to be rinsed with distilled water to avoid undesirable contaminations in the inner tube when taking the density readings for samples.

The same rinsing procedure was also carried out after each blood mimicking fluid sample reading, to rinse the filling tube with water first, followed by rinsing with the next sample solution before taking actual experimental readings. Whenever the filling tube is rinsed with distilled water, a calibration test reading is conducted on the density of distilled water and the density reading will be compared to the standard water density calibration table available in the Anton Par DMA 35 handbook, by checking for the density value of water at the actual measured temperature and compare the deviation with the actual density reading.

When carrying out the density measurement on the blood mimicking fluid samples, the room temperature is controlled at a constant 25 °C in

order to replicate the temperature conditions of a laboratory and simulation environment. To ensure accurate measurement readings, the density measurement procedure will be conducted a minimum of three times to obtain each reading's information and average results for all samples.

v. Viscosity Measurement

The HAAKE MARS Modular Advanced Rheometer was utilized to measure the apparent viscosity of each blood mimicking fluid samples when subjected to shear rates and increasing rotational speed, and rheological characterization of Newtonian and non-Newtonian fluids. The rheometer studies the relationship between the shear stress and strain of the blood mimicking fluid samples in order to determine the deformation behaviour of the varying composition samples.

Prior to starting the rheological sample testing, the appropriate geometries for the rotor head, adapter and specimen cup holder were cleaned and adjusted on the rheometer testing platform, which in this experiment, Rotor CC26 Ti, TMPXX Adapter and TM-PE-C Cup CC CB26 DIN were employed. Next, the RheoWin Job Manager software was booted in the rheometer configured computer, to set up the testing parameters and settings.

All blood mimicking fluid samples were tested at a controlled temperature of 25 °C in order to replicate a surgical simulation environment, with the viscosity test running with a shear rate range of 0.1-1000 s-1, with a divided number of 100 interval readings from the specified range. After setting up the geometry attachments and test simulation settings, the rheometer was calibrated once per usage of the rheometer by readjusting the zero-level point of the measuring rotor via command on the RheoWin software. Once the zero-level point was achieved, the measuring rotor was lifted up so that the specimen cup holder can detached from the measuring platform and filled with 10 mL of the blood mimicking fluid sample to be tested. With the sample specimen in place, the measuring rotor was commanded to go to the inputted gap, which in this case was set as 1 mm as the selected geometric rotor plate comes into contact with the sample fluid.

The measurement was started, and the rotor began to rotate at an increasing rotational speed to compute the viscosity measurement at the stated shear rate range. Concurrently, the RheoWin Data Manager software's integrated server will begin the data plotting of viscosity

against shear rate based on real time responding measurements relayed by the rheometer. For each sample run, the duration of the simulation test taken for the specified shear rate range with 100 intervals was 10 minutes. To ensure accuracy is not compromised, each blood mimicking fluid sample were tested on a triplicate basis. The computed results were tabulated to plot viscosity against shear rate graph for studying the effect of surfactant towards viscosity and viscosity comparison with human blood.

3.0 RESULTS AND DISCUSSION

i. Density Measurement of Blood Mimicking Fluid Samples

Table 3 showcases the average densities for all blood mimicking fluid samples that were computed from triplicate density readings of each individual blood mimicking fluid sample. The ideal density for blood mimicking fluid formulation is given as 1.050±0.040 kg/m^3 by IEC 1685 and shall be taken as comparison to the densities of blood mimicking fluid samples formulated in this experiment.

Table 3: Average density

Sample Set	Samples	Components	Average Densities (g/cm^3)
A	A1	Water: Glycerol	1.0991±0.0001
B	B1	Water: Glycerol: SA	1.1123±0.0004
	B2		1.104±0.0009
	B3		1.1124±0.0008
	B4		1.1115±0.0008
C	C1	Water: Glycerol: XG:SA	1.0951±0.0001
	C2		1.0983±0.0003
	C3		1.0986±0.0004
	C4		1.0989±0.0003
	C5		1.0901±0.0012
D	D1	Water: Glycerol: XG: CS: SA	1.0976±0.0004
	D2		1.0971±0.0002
	D3		1.0974±0.0001
	D4		1.0939±0.0016
	D5		1.0970±0.0007
E	E1	Water: Glycerol: XG:CS:CA:SA	1.1093±0.0002
	E2		1.1088±0.0001
	E3		1.1091±0.0002
	E4		1.1090±0.0003
	E5		1.1123±0.0005

Sample C5 exhibits the closest density to the IEC 1685 specification of 1.0901 g/cm3. Sample E2 exhibits an average density of 1.1088 g/cm3 which is the closest out of the other four set E samples with the density value state by IEC 1685. In terms of the effect of Synperonic A (SA) surfactant concentration, it can be generally interpreted from Table 3 that the blood mimicking fluid samples containing increasing amount of surfactant does not deviate much from their corresponding sample set's fixed blood mimicking fluid sample without surfactant added.

The overall result interpretation on the effect of surfactant towards density is blood mimicking fluid is considered negligible changes from the increasing addition of surfactant. As mentioned in previous section of this paper, Oglat et al. also reported the proposed blood mimicking fluid not influenced by the non-ionic surfactant added, with the highest blood mimicking fluid density reading measured at 1.015 g/cm3 [8]. This may be due to the water-glycerol based fluid making up a significant percentage of the blood mimicking fluid samples composition (97-99.49 wt%), so any addition of chemicals will not have significant influence on the overall density of the blood mimicking fluid.

ii. Viscosity Measurement of Water-Glycerol Base Fluid

Figure 1 graphically depicts the relationship between apparent viscosity and shear rate plot with respect to the power law equation in Equation 1.

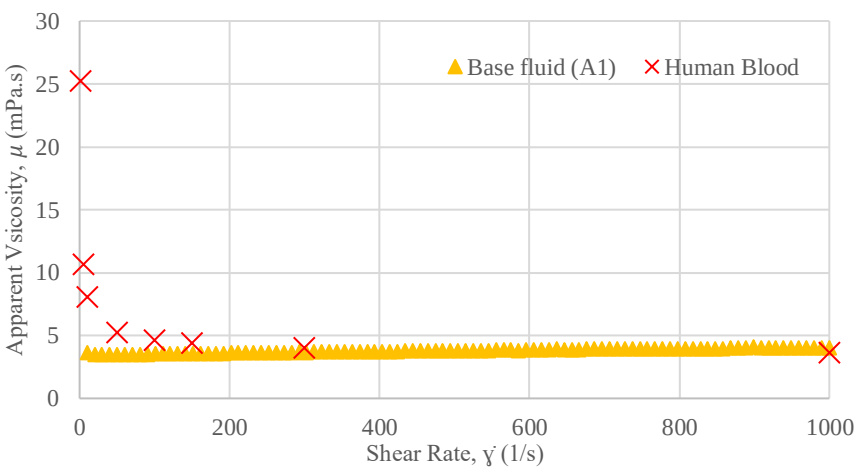

Figure 1: Apparent viscosity against shear rate for water-glycerol base fluid and human blood [5]

It can be observed that the base fluid has an almost linear relationship between viscosity and shear rate, with slight increase in viscosity with increasing shea rate. The slight increase in viscosity throughout the shear region of 0-1000 s-1 may be due to the initial low zero shear viscosity of the base fluid and the extremely slow starting rotational speed of the measuring rotor subjected on the fluid, as it increased to its supposedly stable viscosity range with the increasing shear rate. Nevertheless, it is still indicated that the base fluid viscosity is independent of the influence by increasing shear rate. In other words, the base fluid exhibits Newtonian fluid properties, with the average constant viscosity experimentally determined as 3.7794±0.1683 mPa.s. On the contrary, the human blood can be clearly observed as a non-Newtonian fluid exhibiting pseudoplastic shear-thinning characteristics, as the apparent viscosity decreases with increasing shear rate in a logarithmic manner. Therefore, it is graphically shown that the conventional water-glycerol base fluid was not mimicked the ideal shear-thinning ability of human blood [5].

iii. Viscosity Measurement of Water-Glycerol Base Fluid Samples at varying Surfactant Concentrations

Figure 2 graphically depicts the viscosity against shear rate plot for blood mimicking fluid water-glycerol base fluid samples containing 0 wt% surfactant (A1), 0.5 wt% surfactant (B1), 0.9 wt% surfactant (B2), 1.5 wt% surfactant (B3) and 2.0 wt% surfactant (B4) respectively, and for human blood. The most notable observation is the overall apparent viscosity of the blood mimicking fluid base fluid increased with the higher amount of surfactant added into the sample composition, as sample B1 containing 0.5 wt% surfactant was found to achieve an average apparent viscosity of 5.5894±0.1577 mPa.s with increasing shear rate as compared to the average apparent viscosity of default base fluid at 3.7794±0.1683 mPa.s.

The apparent viscosities were increasingly higher for sample B2, B3 and B4, with sample B4 showcasing the highest viscosity readings relative to shear rate. Therefore, it is interpreted that the addition of surfactant increases the viscosity of the blood mimicking fluid base fluid, as this can be explained by the surfactant's critical micelle concentration (CMC) parameter. The rapid increase in viscosity from each subsequent sample with higher surfactant concentration is mainly due to the increasing micelles formed by the surfactant in the mixture, which exceeded the surfactant's CMC and the formation of visible bubbles suspended in the fluid [11]. As a result, the increasing volume

fraction of bubbles suspended in the base fluid increases the overall viscosity of the base fluid.

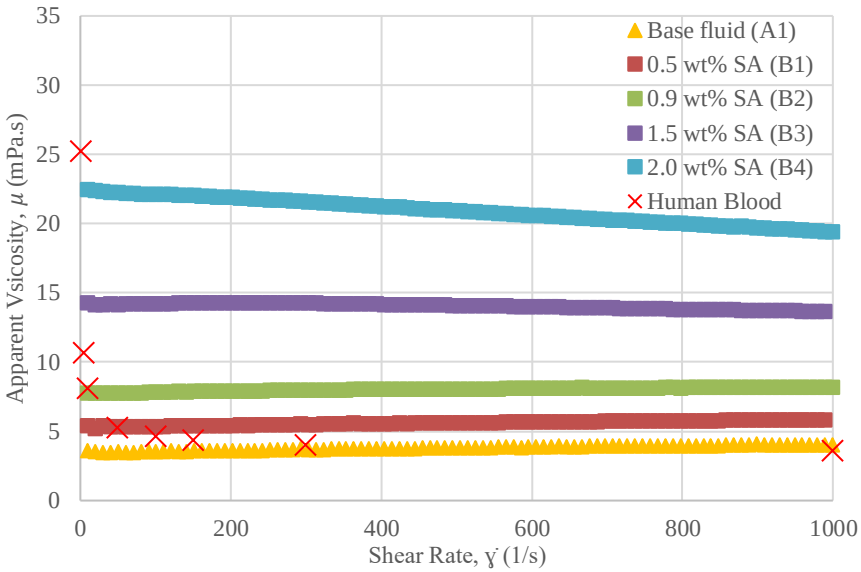

Figure 2: Apparent viscosity against shear rate for water-glycerol base fluid samples with varying surfactant concentrations, and for human blood [5]

In terms of rheological observation, sample B1, B2 and B3 portrayed Newtonian fluid characteristics closely that are similar to the water-glycerol base fluid, with slight fluctuations in viscosities due to the significantly low stating rotational speed subjected during rheometer testing. However, sample B4 containing the highest surfactant concentration of 2.0 wt% surfactant exhibits a sharp shear-thinning behaviour as the apparent viscosity decreases with increasing shear rate, labelling it a non-Newtonian fluid.

The abnormal shear-thinning characteristic associate with a supposedly Newtonian base fluid is due to the micelles suspended in the base fluid that can influence the rheological properties to be different, from Newtonian to non-Newtonian [11]. This statement is supported with the CMC principles, as the increasing micelles formed exceeded CMC limit, the oversaturation of micelles in the base fluid

resulted with the presence of free micelles that does not interact with the blood mimicking fluid component molecules present. Therefore, the presence of free micelles increases the free water suspension in the base fluid and significantly decrease the overall viscosity of the base fluid [12]. In terms of similarity with real human blood, it is visibly clear that the sample with the closest viscosity with human blood (Sample A1) wasn't able to exhibit the shear thinning behaviour of blood. Indeed, Sample B4 exhibited shear-thinning behaviour but the degree of shear-thinning is not to the same extent of a human blood, not to mention its overall viscosity range is too high to match with the viscosity of human blood.

iv. Viscosity Measurement of Blood Mimicking Fluid Samples with Xanthan Gum at varying Surfactant Concentrations

Figure 3 shows the viscosity against shear rate plot for blood mimicking fluid samples comprising of the base fluid with XG and varying concentration of surfactant mixed, and for actual human blood [5].

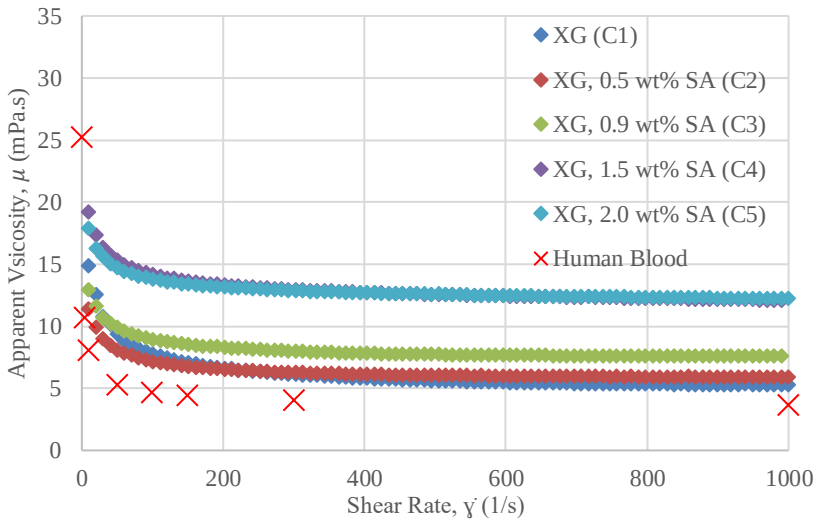

Figure 3: Apparent viscosity against shear rate for blood mimicking fluid samples containing xanthan gum with varying surfactant concentrations, and for human blood [5]

It is observable that all five of the specified samples are exhibiting similar degree of shear-thinning behaviour of a non-Newtonian, pseudoplastic fluid with the apparent viscosities decreasing with shear rate until they reach a lower viscosity plateau at higher shear region, in

which a Newtonian fluidic behaviour is observed.

The shear-thinning properties observed are contributed by the presence of xanthan gum in the sample mixtures. Similar case with the results obtained from Figure 2, the overall viscosities of the blood mimicking fluid samples shown in Figure 3 increases with each subsequent sample with higher surfactant concentration. This can be explained based on the application of surfactant that is responsible for dispersing the blood mimicking fluid component particle (XG) in the base fluid for homogeneity, thus increasing the overall viscosity of the blood mimicking fluid.

The viscosity difference between sample C4 and C5 containing 1.5 wt% and 2.0 wt% respectively is noted to be insignificant, in which sample C4 with lower surfactant concentration of the two showcases higher viscosity in the lower shear region of 0-400 s-1 and sharper decrease in viscosity in the higher shear region onwards. This can be explained as the limitation of the surfactants CMC, as the generation of micelles interacting with other blood mimicking fluid component particles from the high surfactant concentration added in sample C4 occurs at a higher formation rate, this leads to an increase in the overall viscosity and also the rate of free micelles formed. Hence, the increasing saturation of free micelles in the sample mixture causes a significant decrease in viscosity of the blood mimicking fluid sample [12].

Based on the results of Figure 2 and 3, it is concluded that the non-ionic surfactant used for this experiment increases the viscosity for both Newtonian and non-Newtonian fluids. From Figure 3, sample C2 with 0.5 wt% surfactant showcases a shear-thinning trend and apparent viscosity of the highest similarity out of all Set C samples with human blood in the lower shear region of 0-200 s-1. At higher shear rates, the sample without surfactant addition (C1) portrays the most similar shear-thinning gradient and viscosity range with human blood.

v. Viscosity Measurement of Blood Mimicking Fluid Samples with Xanthan Gum and Corn Starch at varying Surfactant Concentrations

Figure 4 depicts the relationship between viscosity and shear rate of blood mimicking fluid samples containing 0.01 wt% XG, CS each with the addition of varying surfactant concentrations, and for human blood.

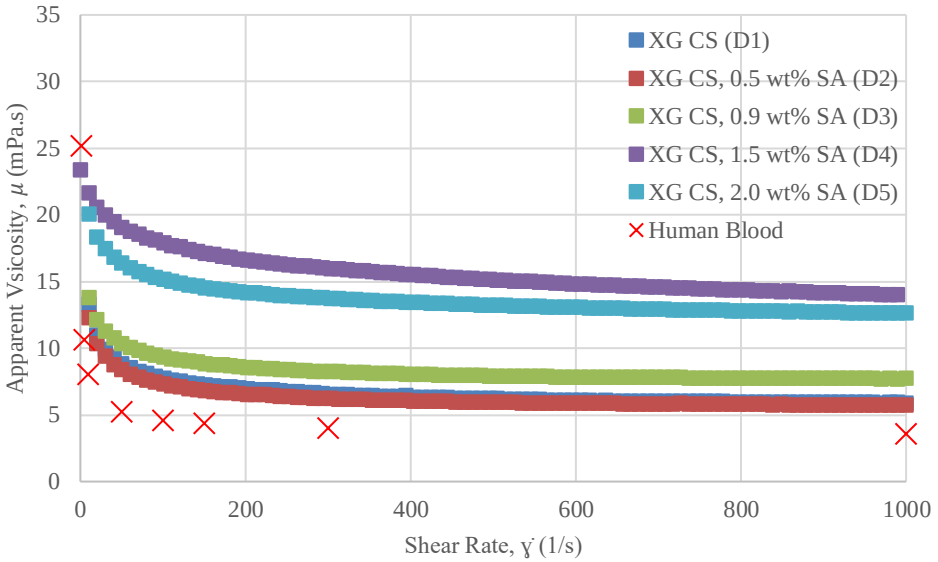

Figure 4: Apparent viscosity against shear rate for blood mimicking fluid samples containing xanthan gum and corn starch with varying surfactant concentrations, and for human blood [5]

Comparing Figure 3 and Figure 4, it is visibly clear that the overall viscosity results of the Set D samples plotted in Figure 4 are higher than Set C samples in Figure 3. That is due to the addition of CS into the blood mimicking fluid samples which is capable of synergizing the intermolecular interactions with XG as polysaccharides, creating more significant viscosity effect [13].

Based on Figure 4, it is observed that the overall viscosity of the blood mimicking fluid sample with the lowest surfactant added of 0.5 wt% surfactant (D2) is lower than the sample without surfactant added (D1). The overall viscosity of the subsequent sample with 0.9 wt% surfactant (D3) increased higher than sample D1 and D2, followed by a significant increase in viscosity for the subsequent sample D4 with higher surfactant concentration. However, the sample with the highest surfactant concentration added of 2.0 wt% (D5) is observed to portray a relatively lower overall viscosity than sample D4.

The results from Figure 4 does not validate that increasing surfactant concentration will necessarily result with an increase in viscosity under increasing shear rates. For the case of sample D4 and D5, in can be similarly deduced like the previous case with sample C4 and C5, which

the degree of free micelles saturation in the sample D5 is higher than in sample D4, leading to a significant decrease in overall viscosity of sample D5. As for the decrease in overall viscosity from non-surfactant sample D1 to sample D2, this result occurrence may be linked to the intermolecular interactions aspect of the blood mimicking fluid formulation, in which the surfactant's role in the two blood mimicking fluid sample compositions have different effect on the rheological properties.

All five blood mimicking fluid samples plotted in Figure 4 exhibits good shear-thinning characteristics. For sample D4 however, a strong shear-thinning behaviour is observed for the shear rate region of 200 to 1000 s-1, which deviates from human blood as it should be more Newtonian-like at high shear rates, showing a slightly linear viscosity to shear rate trend. Goncalves et al. also reported a similar finding in which a very high surfactant concentration used in blood mimicking fluid resulted with a shear-thinning trend that deviates greatly from the shear-thinning graph of human blood [7].

Out of all the five samples in Figure 4, sample D2 containing 0.01 wt% of XG, 0.01 wt% of CS and 0.5 wt% of surfactant mimics the overall viscosity from 0-1000 s-1 and the shear-thinning pattern of human blood with the highest similarity by far.

vi. Viscosity Measurement of blood mimicking fluid Samples with Xanthan Gum, Corn Starch and Contrast Agent at varying Surfactant Concentrations

Figure 5 depicts the relationship between viscosity and shear rate for blood mimicking fluid samples containing 0.01 wt% XG, CS each, with the addition of 10 ml of CA and varying surfactant concentrations, and for human blood. Similar to the case of sample D1 and D2 that was previously discussed, the overall viscosity of the blood mimicking fluid sample with 0.5 wt% surfactant (E2) is observed to be lower than the non-surfactant added sample (E1), according to Figure 5.

The overall viscosity for the remaining three samples increases with the higher amount of surfactant added for their respective composition, with the sample added with 2.0 wt% surfactant portraying the highest overall viscosity out of Set E samples. Furthermore, it is evidently clear that all five blood mimicking fluid samples exhibits obvious shear-thinning characteristics of a pseudoplastic fluid, with the exception of

sample E2. Although sample E2 has an overall viscosity that is most similar to that of the human blood, its composition exhibits a weak shear-thinning pattern around the shear rates of 0-200 s-1, followed by a slightly resembling linear Newtonian viscosity-shear rate trend at higher shear rates onward.

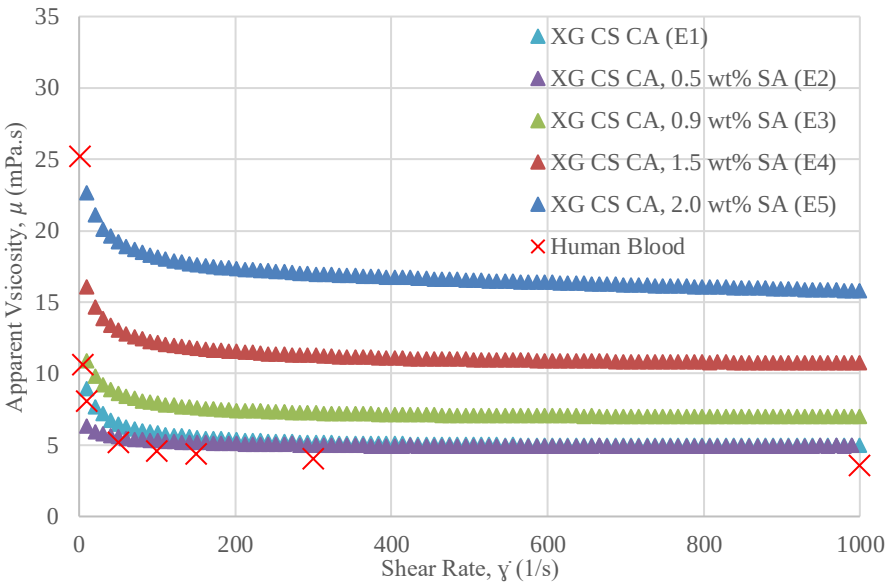

Figure 5: Apparent viscosity against shear rate for blood mimicking fluid samples containing xanthan gum, corn starch and contrast agent with varying surfactant concentrations, and for human blood [5]

According to a study on the effect of contrast media conducted by Pugh [14], it was reported that iodinated contrast media has the ability to produce rheological alterations when injected into a non-Newtonian blood, primarily due to the viscosity and osmolality difference between the contrast media and blood. Hence, it can be interpreted that the CA added in Set E samples has shear-thickening properties which might have reduced the overall shear-thinning ability of the blood mimicking fluid samples.

4.0 CONCLUSION

The addition of non-ionic surfactant does not have any significant effect on the densities of the various blood mimicking fluid compositions comprising of water-glycerol base fluid, xanthan gum, corn starch and contrast agent.

The water-glycerol based fluid makes up a large percentage of the blood mimicking fluid samples composition so other constituents added into the blood mimicking fluid composition will not have significant influence on the overall density of the blood mimicking fluid. On the other hand, the addition of non-ionic surfactant affected the apparent viscosity of blood mimicking fluid formulations. In general, the higher the surfactant concentration added into the blood mimicking fluid, the higher the overall viscosity of the blood mimicking fluid. High surfactant concentration of greater than 2 wt% in blood mimicking fluid was found to grant the Newtonian base fluid shear thinning characteristics with viscosity decreasing as the shear rate increases and increases the shear-thinning properties of blood mimicking fluid. According to the viscosity profile, the blood mimicking fluid containing 59.48 wt% water, 40 wt% glycerol, 0.01 wt% xanthan gum, 0.01 wt% corn starch, 4vol/wt % contrast agent and 0.5 wt% of surfactant showcases the closest viscosity profile with the actual human blood. It is recommended to further investigate the rheologcal properties by comparing with blood rheological models .

5.0 ACKNOWLEDGMENTS

This work would not have been possible without the financial support provided by Ministry of Higher Education Malaysia under Fundamental Research Grant Scheme (FRGS/1/2020/TK0/TAYLOR/02/5). The authors also would like to acknowledge the research material received from Croda Singapore Pte Ltd.

6.0 REFERENCES

[1] S. Maroni, V. Mauri, E. Negrello, L. Pugliese, A. Pietrabissa and F. Auricchio, "Quantitative assessment of 3D printed blood vessels produced with J750™ digital anatomy™ for suture simulation," 2022, doi: 10.1101/2022.01.09.475308.

[2] A. Pietrabissa, S. Marconi, E. Negrello, V. Mauri, A. Peri, L. Pugliese, E. M. Marone, and F. Auricchio, "An overview on 3D printing for abdominal surgery," *Surgical Endoscopy*, vol. 34, no. 1, pp. 1–13, 2019.

[3] T. A. Fuhrmann, A. Schlesinger, M. Schultz, and K-V. Jenderka, "Blood Mimicking Fluid for Reproducing Rheological and Acoustical Blood Properties," *Proceedings of the 46th Annual Ultrasonic Industry Association*

Symposium, 2017.

[4] M. Z. Matjafri, A. A. Oqlat, N. Suardi, M. A. Oqlat, M. A. Abdelrahman, and A. A. Oqlat, "A review of suspension-scattered particles used in blood-mimicking fluid for Doppler ultrasound imaging," *Journal of Medical Ultrasound*, vol. 26, no. 2, p. 68, 2018.

[5] J. M. Jung *et al.*, "Reference intervals for whole blood viscosity using the analytical performance-evaluated scanning capillary tube viscometer," *Clin. Biochem.*, vol. 47, no. 6, pp. 489–493, 2014, doi: 10.1016/j.clinbiochem.2014.01.021.

[6] X. Zhou and P. R. Hoskins, "Testing a new surfactant in a widely-used blood mimic for ultrasound flow imaging," *Ultrasound*, vol. 25, no. 4, pp. 239–244, 2017.

[7] I. Gonçalves, J. Varelas, G. Coutinho, A. Moita, D. Pinho, R. Lima, J. Miranda, E. Veja, J. Montanaro, and A. Moreira, "Dynamic flow behaviour of a blood analogue fluid in microchannels for microcirculation studies," *Proceedings of the 14th International Joint Conference on Biomedical Engineering Systems and Technologies*, 2021.

[8] A. A. Oglat, M. Z. Matjafri, N. Suardi, M. A. Oqlat, A. A. Oqlat and M. A. Abdelrahman, "A New Blood Mimicking Fluid using Propylene Glycol and their Properties for a Flow Phantom Test of Medical Doppler Ultrasound ," *International Journal of Chemistry, Pharmacy & Technology*, vol. 2, no. 5, pp. 220–231, 2017.

[9] N. Perrira, A. S. Shuib, S. W. Phang and A. S. Muda, "The Formulation of Blood Mimicking Fluid for Application in Medical Simulator under Angiography Visualisation," *B.S. Thesis*, School of Engineering, Taylor's University, Selangor, 2021.

[10] "Omnipaque (Iohexol Injection): Uses, Dosage, Side Effects, Interactions, Warning." https://www.rxlist.com/omnipaque-drug.htm (accessed October 18, 2022).

[11] E. Rosenbaum, M. Massoudi, and K. Dayal, "Surfactant stabilized bubbles flowing in a newtonian fluid," *Mathematics and Mechanics of Solids*, vol. 24, no. 12, pp. 3823–3842, 2019.

[12] N. C. Crawford, L. B. Popp, K. E. Johns, L. M. Caire, B. N. Peterson, and M. W. Liberatore, "Shear thickening of corn starch suspensions: Does concentration matter?," *J. Colloid Interface Sci.*, vol. 396, pp. 83–89, Apr. 2013, doi: 10.1016/J.JCIS.2013.01.024.

[13] Annu and S. Ahmed, "Advanced green materials: An overview," *Advanced Green Materials*, pp. 1–13, 2021.

[14] N. D. Pugh, "Haemodynamic and rheological effects of contrast media: The role of viscosity and osmolality," *European Radiology*, vol. 6, no. S2, 1996.

ESTABLISHMENT OF TYPICAL DOSE VALUE FOR INTERVENTIONAL RADIOLOGY EXAMINATION IN RADIOLOGY DEPARTMENT, HOSPITAL PENGAJAR UPM

A.A. Zurihanaz and N.M. Noor[1,2,*]

[1]Medical Physics Unit, Hospital Pengajar Universiti Putra Malaysia, 43400 Serdang, Selangor, Malaysia.

[2]Medical Physics Laboratory, Department of Radiology, Faculty of Medicine and Health Sciences, 43400 Serdang, Selangor, Malaysia

[*]Corresponding Author's Email: noramaliza@upm.edu.my

Article History: Received January 24, 2023; Revised January 26, 2023; Accepted January 26, 2023

ABSTRACT: Angiography is commonly used as a diagnostic imaging tool for diagnosing and treating the patient from simple to complex examination. Despite the advancement in imaging technologies, the radiation dose to the patient remains a concern when using this procedure. Diagnostic Reference Levels (DRLs) are used to identify the amount of dose exposed to the patient and monitor the high dose received by an individual in a specified radiological procedure. The aim of this study is to establish Institutional Diagnostic Reference Levels (DRLs) based on median data dose distribution for cerebral examination (cerebral angiography and stroke thrombectomy) and compared with established Malaysian National Diagnostic Reference Levels (MNDRLs). The Dose Area Product (DAP) and fluoroscopy time were recorded using clinical data from the participating modality from 1 January 2022 until 31 December 2022 at Teaching Hospital Universiti Putra Malaysia (HPUPM). The data collected for each procedure with a minimum recommended number of patients (at least 30) required to propose a DRL for each examination type within the data collection period. The mean value, standard deviation, median value, and third quartile were calculated using Microsoft Excel Version 2013. The Typical Dose Value for the interventional procedure was defined as the median of the distribution of DRL quantities and required further optimization. The distribution of DAP values for the cerebral angiogram and stroke thrombectomy ranged between 5.05 mGy.m^2 to 31.80 mGy.m^2 and 7.03 mGy.m^2 to 43.23 mGy.m^2 respectively. The institutional DRLs for cerebral

angiogram (10.60 mGy.m^2) and stroke thrombectomy (21.80 mGy.m^2) were higher than the established MNDRL. From the findings, stroke thrombectomy examinations recorded the highest Typical Dose value follow by cerebral angiogram examination. Generally, the factors that can affect DRL values are a patient-related factor, equipment-related factor, the complexity of the procedures, operator's experience in handling the machine and interventional radiologist experience that can contribute to various results.

KEYWORDS: *Typical Dose Value Diagnostic Reference Level (DRL); Radiation Dosage; Interventional Radiology; Cerebral Procedure, Dose Management*

1.0 INTRODUCTION

Interventional Radiology (IR) is a non-invasive technique that evolved in various fields of medicine including diagnostic and therapeutic procedures for numerous diseases. The use of IR in the Radiology Department tends to increase significant radiation exposure and there is a possibility of increased radiation risks to both patients and staff. According to the Internal Commission of Radiological Protection (ICRP), the absorbed dose threshold for the brain and lens of the eye is as low as 0.5 Gy and the patients could exceed the threshold of tissue reaction when the procedure is very complex and take longer duration time [1]. Therefore, the concern in tissue reaction when the maximum dose of patients reached above the threshold value should be an emphasis on optimisation of unnecessary radiation as well as preventing skin erythema or epilation, cataract and severity of the deterministic effect.

Radiation dose given to patients can be high or low depending on the type of examination, patient size and different techniques used by radiographers and radiologist during interventional procedures. The lack of experience radiologist in interventional procedures might be an important factor affecting increasing fluoroscopic time and patient radiation dose. With the recent advanced technologies, the availability of dose monitoring devices to keep track of patient dosimetric data with numerous parameters used in different modalities and dose management in this facility plays a pivotal role in improving the patient dosage including proper training of fluoroscopic operator and

use various of dose reduction techniques [2].

Diagnostic Reference Level (DRL) is an indicator used to identify the dose to the patient is unusually high or low in a specified radiological procedure for medical imaging equipment [3]. DRLs were determined through the 75th percentile of the distribution of median value and act as a guide for monitoring dose to individual patients meanwhile Typical Dose Value was determined by the median value of the distribution of the DRL quantity, as there are insufficient data to use the third quartile hence require further optimization. Therefore, DRL is not a dose limit, but as a tool for dose optimizations during diagnostic procedures [4]. The ICRP indicates that DRLs are recommended by professional organizations to measure the dose distribution among patients and for local review if regularly exceeded. They recommend considering DRLs as much as possible during all procedures using radiation because the cumulative fluoroscopy exposure time is a poor metric of patient radiation dose [5].

The establishment of DRL is relatively common in simple examinations such as radiographic procedures. In interventional guided examinations, DRLs only applied in the management of patient doses to ensure patient doses are as low as reasonably achievable (ALARA) to avoid unnecessary stochastic effects [6]. However, for complex procedures involving fluoroscopy or CT examinations, establishing a DRL is quite difficult due to the multiple images taken and fluoroscopy time leading to a wide range of DAP dose distribution in different procedures. As a consequence, DRLs are required to evaluate patient dose and as a guided protocol in monitoring exceeding radiation dose.

This work focuses on the establishment of Typical Dose Values for interventional examination. Kerma Area Product (KAP) or Dose Area Product (DAP) is the required primary DRL quantity. DAP is a useful parameter to correlate well using total energy given to a patient, which is associated with the effective dose, therefore to overall cancer risk. The Typical Dose value for interventional procedures is established on the median of local distributions which are then compared with the established MNDRL [7][8]. MNDRL and Typical Dose Value should be

set for each examination or procedure for each clinical indication to provide investigation levels for uncommon practices.

This study aimed to prospectively collect patient radiation doses and help to contribute to facility DRL for common cerebral procedures using the angiography system in the radiology department at HPUPM.

2.0 MATERIALS AND METHODS

2.1 Patient Dose Data

Patient data were collected from 1 January 2022 until 31 December 2022 from the Angiography console (Philips Allura Xper FD20/15) in Radiology Department, HPUPM equipped with a dose tracking system that indicates Diagnostic Reference quantities that have been proposed in Interventional radiology procedures. Dose monitoring devices usually keep track of Total air Kerma-Area Product (PKa,r), Total Dose Area Product (DAP), Total Fluoroscopy Time (FT), Total Number of Images (NI) and type of protocol procedures used. All these quantities represent dosimetric information where PKa,r relates to the effective dose given by accumulated exposure and exhibits subsequent stochastic effect [9][10]. Dose information for each patient was provided in the form of total DAP radiation dose metric and total fluoroscopy time was recorded.

2.2 Data Preparation

A total of 160 patients who participated in this study were cruited having met the following inclusion criteria of all fluoroscopic procedures listed in Guidelines on Malaysian DRLs in Medical Imaging (Radiology). However, two exclusion criteria were not included in this study since there is no Malaysian DRLs value of fluoroscopic procedures on patients below 16 years old and examinations done with fluoroscopy equipment that does not have KAP meter. The subjects were divided into two types of procedures; 129 cerebral angiogram and 31 stroke thrombectomy respectively with minimum recommended number of patients (at least 30) required to propose a DRL for each examination type within the data collection period, based on the recommendation from the ICRP Publication 135

[11]. The data was further analysed to determine the typical dose value and DRLs obtained from total DAP values.

2.3 DRL Calculation and Analysis

The total Dose Area Product (mGy.m^2) and total fluoroscopy time from the dose monitoring device were studied. All the data were analyzed to determine mean value, standard deviation, first quartile, median and third quartile using Microsoft Excel 2013 Version. The results of the data were presented in descriptive statistics of box plots and graphs. The median calculation obtained from the software for two types of interventional procedure represents a typical dose value to be established in Radiology Department, HPUPM. Meanwhile, the third quartile was used for the comparison with internationally established MNDRL. The use of DRL concept and quantities as optimization tools in our facility and was highly recommended by ICRP to reduce the dose as well as prevent unnecessary radiation to patients[12].

3.0 RESULTS AND DISCUSSION

The establishment of Typical Dose Value as a part of DRLs in interventional radiology was discussed further in this section. The DRL is classified according to the examination conducted on an individual obtained from median data known as the Typical Dose Value in data dose distribution. The established MNDRL in our country for cerebral examination (type of procedure not specified) was 8.7 mGy.m^2 and this value has not been revived for over ten years since 2013 [13]. DRLs in our institution have not been established yet and this study presented DRLs for two common procedures in our hospital. The Typical Dose Value contributed significantly to the goal of optimization of radiation doses and required further optimization.

A total of 160 Interventional procedures involving two different cerebral examinations: 129 cerebral angiogram (80.63%) and 31 stroke thrombectomy (19.38%) were collected. The most frequently performed in Interventional Radiology procedures were cerebral angiogram, stroke thrombectomy, cerebral aneurysm, central venogram, central venoplasty, fistulogram, right arthrogram, shoulder arthrogram, antegrade stenting, nephrostomy and permanent catheter. However, a minimum of 30 cases per examination were analyzed in

this study.

Table 1 presents descriptive statistics for the DRL quantities (mean value, standard deviations, median value and 75th percentile) for cerebral angiogram and stroke thrombectomy respectively. Figure 1 presents (in the form of box plots) the distribution of each DRL quantity (DAP and fluoroscopy time) for both cerebral procedures. Figures 2 and 3 present the Typical Dose Value, 75th Percentile and established MNDRL.

The distribution of DAP values (Figure 1) for cerebral angiogram and stroke thrombectomy were ranged between 5.05 mGy.m² (min) to 31.80 mGy.m² (max) and 7.03 mGy.m² (min) to 43.23 mGy.m² (max) respectively. On the other hand, the distribution of fluoroscopy time ranged between 3.14 minutes (min) to 52.42 minutes (max) and 5.10 minutes (min) to 117.02 minutes (max) respectively. From the results, Stroke Thrombectomy was the one that delivered the highest doses to patients and required the highest fluoroscopy times. The relatively high dose received by the patient in interventional procedure due to the complexity of examination and the total number of images taken. The observation of the complexity of cases could be due to different radiologist experience with the different techniques used during the procedure. In addition, high fluoroscopy time may be elucidated by the use low of pulse-rate fluoroscopy. Meanwhile, the elevated number of images taken could be the inconsistency in the interpretation of these specific images by radiologist and require further investigation in specific cases.

Table 1: Descriptive Statistics and Typical Dose Value for Cerebral Examination

DRL Quantities	Total DAP (mGy.m²)			Total Fluoroscopy Time (min)		
	Mean (SD)	Median	75th Percentile	Mean (SD)	Median	75th Percentile
Cerebral Angiogram	11.26 (4.17)	10.60	13.10	14.89 (10.23)	11.21	19.30
Stroke Thrombectomy	21.41 (6.48)	21.80	24.30	42.41 (22.45)	40.07	52.38

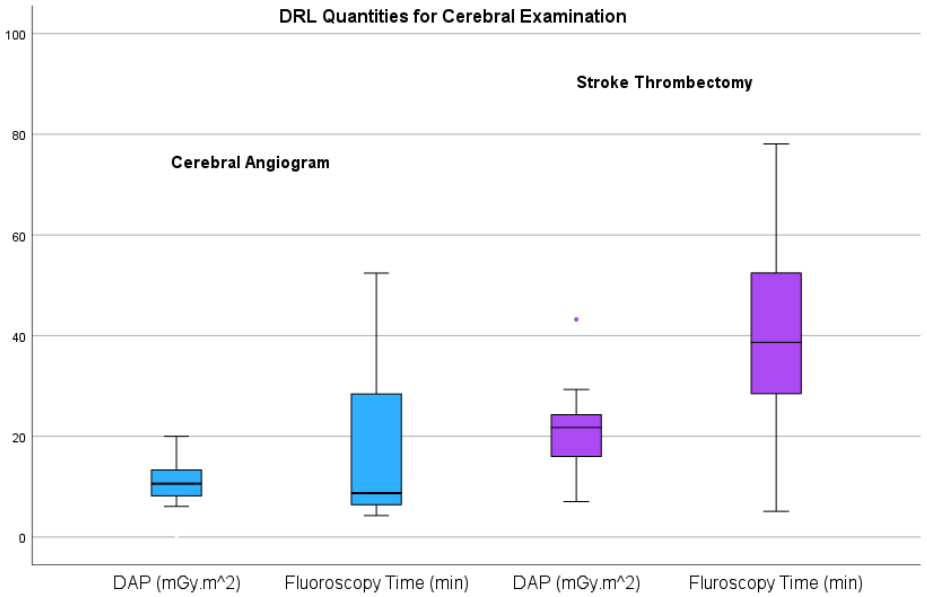

Figure 1: Box Plots of The Distributions of each DRL Quantities

Figures 2 and 3 show the Typical Dose Value (based on median values), 75th Percentile and Established MNDRL (based on dose summation of a single region) for both cerebral angiogram and stroke thrombectomy. The findings, show that the Typical Dose Value for cerebral angiogram (10.60 mGy.m^2) and stroke thrombectomy (21.80 mGy.m^2) are higher than the national DRL. Since the MNDRL was not revived yet, we are now using Typical Dose Value in our hospital for both cerebral procedures. Generally, the factors that can be affect DRL values are patient age, weight, scanning time, efficiency of the equipment and the operator's experience in handling the machine that can contribute to various effects.

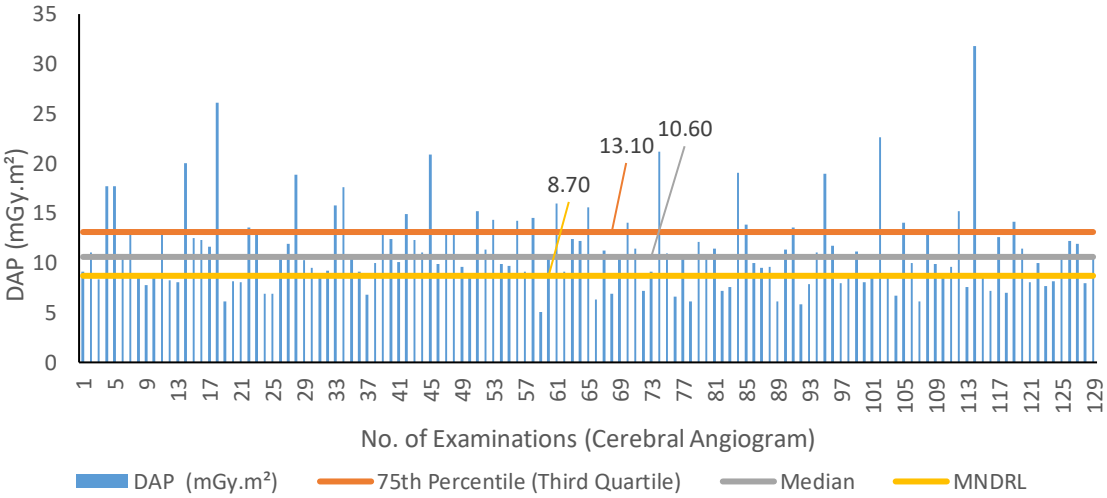

Figure 2: The Typical Dose Value (Median), 75th Percentile and MNDRL for Cerebral Angiogram

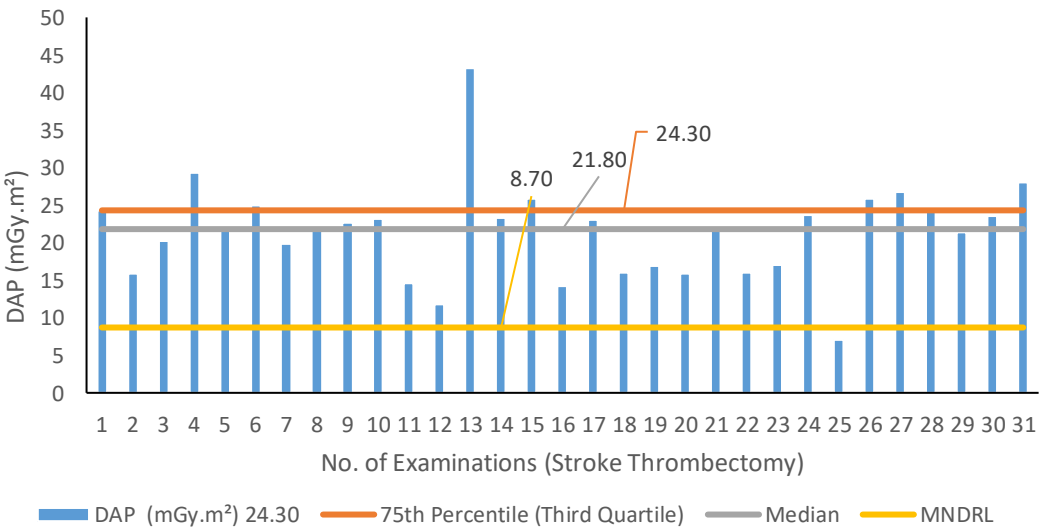

Figure 3: The Typical Dose Value (Median), 75th Percentile and MNDRL for Stroke Thrombectomy

4.0 CONCLUSION

Institutional DRLs were established using the median value for two types of examination (cerebral angiogram and stroke thrombectomy). The typical dose value for cerebral angiogram and stroke thrombectomy was 10.60 mGy.m^2 and 21.80 mGy.m^2 respectively. The Typical Dose value was higher than the established MNDRL. The complexity of the procedure was found in stroke thrombectomy where the patient dose was relatively high which can cause tissue reaction when the dose reaches a threshold value. The concept of As Low as Reasonably Achievable (ALARA) and dose management should be implemented in this hospital without affecting the image quality.

5.0 ACKNOWLEDGMENTS

We acknowledge the facilities use in the Medical Physics Unit of HPUPM for the data collection from the Angiography system. This research did not receive any specific grant or funding from the government or other agencies.

6.0 REFERENCES

[1] Boal, T. J., & Pinak, M. (2015). Dose limits to the lens of the eye: International basic safety standards and related guidance. *Annals of the ICRP*, *44*, 112–117.

[2] Mahadevappa, M. (2001). Fluoroscopy: Patient radiation exposure issues. RadioGraphics. Vol 21 Issues 4 (1022-1045)

[3] International Atomic Energy Agency. (2017, August 1). Radiation Protection in Fluoroscopy.

[4] Erskine J. Brendan, Zoe Brady & Elissa M. Marshall. (2014). Local Diagnostic Reference Levels for Angiographic and Fluoroscopic Procedures: Australian Practice. *Australas Phys Eng Sci Med.* 37:75-82.

[5] Hayashi, S., Takenaka, M., Hosono, M., Kogure, H., Hasatani. (2021). Diagnostic reference levels for fluoroscopy-guided gastrointestinal procedures in Japan from the rex-gi study: A nationwide multicentre prospective observational study. *SSRN Electronic Journal*.

[6] International Atomic Energy Agency. (2014). Radiation Protection and Safety of Radiation Sources: International Basic Safety Standards. *IAEA*

Safety Standards Series No. GSR Part 3.

[7] International Atomic Energy Agency. (2017, August 7). *Radiation doses in interventional procedures*. IAEA. Retrieved January 28, 2023, from https://www.iaea.org/resources/rpop/health-professionals/interventional-procedures/radiation-doses-in-interventional-fluoroscopy

[8] Bleeser, F., Hoornaert, M.-T., Smans, K., Struelens, L., Buls, N., Berus, D., Clerinx, P., Hambach, L., Malchair, F., & Bosmans, H. (2008). Diagnostic reference levels in angiography and Interventional Radiology: A Belgian multi-centre study. *Radiation Protection Dosimetry*, *129*(1-3), 50–55.

[9] Tsapaki, V. (2020). Radiation dose optimization in Diagnostic and interventional radiology: Current issues and future perspectives. *Physica Medica*, *79*, 16–21.

[10] Papanastasiou, E., Protopsaltis, A., Finitsis, S., Hatzidakis, A., Prassopoulos, P., & Siountas, A. (2021). Institutional diagnostic reference levels and peak skin doses in selected diagnostic and therapeutic interventional radiology procedures. *Physica Medica*, *89*, 63–71.

[11] Vañó, E., Miller, D. L., Martin, C. J., Rehani, M. M., Kang, K., Rosenstein, M., Ortiz-López, P., Mattsson, S., Padovani, R., & Rogers , A. (2017). ICRP publication 135: Diagnostic Reference Levels in medical imaging. *Annals of the ICRP*, *46*(1), 1–144.

[12] International Commission on Radiological Protection. (2017). Diagnostic Reference Levels in Medical Imaging. Vol 46. No 1. ISSN 0146-645.Ministry of Health. 2013. Malaysian Diagnostic Reference Levels in Medical Imaging (Radiology). Radiation Health and Safety Section.

[13] Ministry of Health. (2013). Malaysian Diagnostic Reference Levels in Medical Imaging (Radiology). Radiation Health and Safety Section.

A REVIEW OF CLASSIFICATION TECHNIQUES FOR ELECTROMYOGRAPHY SIGNALS

S.N. Omar[1], N.M. Saad[2,*], A.R. Abdullah[3], E.F. Shair[4], H. Rashid[5]

[1,3,4]Faculty of Electrical Engineering,Universiti Teknikal Malaysia Melaka, Malaysia.

[2]Faculty of Electrical & Electronic Engineering Technology, Universiti Teknikal Malaysia Melaka, Malaysia.

[5]Motorcycle Engineering Technology Lab (METAL), Faculty of Mechanical Engineering, Universiti Teknologi MARA, Shah Alam,Malaysia.

[*]Corresponding Author's Email: norhashimah@utem.edu.my

Article History: Received January 16, 2023; Revised January 25, 2023; Accepted January 25, 2023

ABSTRACT: Electromyography (EMG) signals can be used in various sector such as medical, rehabilitation, robotics, and industrial fields. EMG measures muscle response or electrical activity in response to a nerve's stimulation of the muscle. To detect neuromuscular abnormalities, these test is very useful. EMG can measures the electrical activity of muscle during rest, slight and forceful contraction. Normally, during rest our muscle tissue does not produce electrical signals. Machine Learning (ML) is an area of Artificial Intelligent (AI) with a concept that a computer program can learn and familiarize to new data without human intervention. ML is one of major branches of AI. Aim for this paper is to recover the latest scientific research on ML methods for EMG signal analysis. This paper focused on types of ML classifiers that are suitable for analysis the EMG signal in terms of accuracy. During the content review, we understood that ML performed for big and varied datasets. All of the ML classifiers have their own algorithm, special specification, pros and cons based on the available input. In this review revealed that Support Vector Machine (SVM), K-Nearest Neighbor (KNN) and Linear Discriminant Analysis (LDA) are most popular algorithms in ML that used in diagnosis of EMG signal especially for upper limbs of our body because mostly the accuracy for the respective classifier shows that more than 80 to 90% accurate results. This article depicts the application of various ML algorithms used in EMG signal analysis till recently, but in the future, it will

be used in more medical fields to improve the quality of diagnosis.

KEYWORDS: *Electromyography; Machine Learning; Classification*

1.0 INTRODUCTION

Surface electromyography, often known as sEMG, is a technique that is used to assess the electrical activity of a muscle in a non-invasive manner by placing surface electrodes on the skin at sufficient positions [1]. When flexing or extending an articulation, it can assist in retrieving muscle information during contractions. In addition, there are implants that can be inserted beneath the skin to assist with signal acquisition; however, these are not commonly used [2]. To perform pattern recognition for EMG applications, features can be extracted from sEMG signals and analyzed. The signal analysis can be performed in time domain or by using other domains, including the frequency domain (also known as the spectrum domain), time scale, and time–frequency, among others.

Machine Learning (ML) is an Artificial Intelligence (AI) applications that using mathematical algorithms to learn and interpret patterns without direct instruction. There are many ML algorithms that have been proposed as classification technique for pattern recognition. In sEMG signal analysis, the popular techniques include Support Vector Machines (SVM), Linear Discriminant Analysis (LDA), K-nearest-neighbour's (KNN) and Naïve Bayes (NB). Each of the classifier have their own potential to recognize complex patterns in sEMG signals.

2.0 ELECTROMYOGRAPHY (EMG)

Electromyography (EMG) is an electrical signal analysis to evaluate muscle activities by detecting electrical potential signals generated by muscle cells [3]. Since EMG signals provide more information on the activity of the muscle, this technique has also emerged as the gold standard for identifying muscular tiredness [4]. Surface electromyography (sEMG) is a scientific tool used to quantify muscle activity of workers during prolonged standing tasks. [5]. It can be measured by two methods: (a) applying electrodes to the skin surface (non-invasive) or (b) intramuscular (invasive) within the muscle [6]. Both methods are shown in Figure 1.

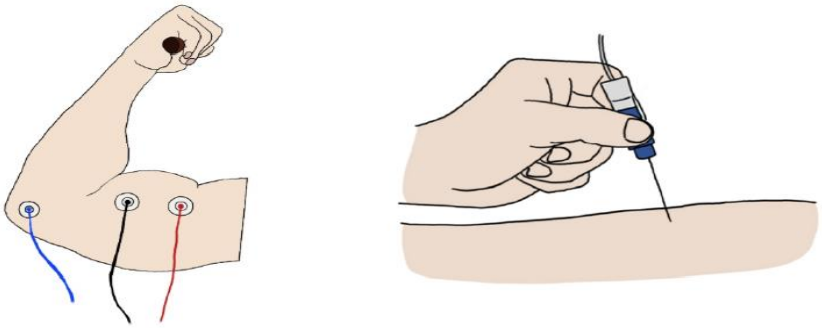

(a) **(b)**

Figure 1 : (a) Image of surface Electromyography(sEMG) or non-invasive electrode and (b) Needle Electromyography or invasive electode [7]

sEMG is more extensively employed because of its significant stability advantage. However, because needle EMG involves physically inserting a needle into the muscle, it provides more reliable data than sEMG. As a result of studying the relationship between the trigger point and the central nervous system to discover issues connected with muscle pain syndrome and conducting EMG-based research, the necessary EMG could not be detected using surface recording techniques. [7]. Electromyography have some phenomena [8] or it can call spontaneous activity that consists of Fibrillation, Fasciculation, Myotonia, Neuromyotonia and Myokymia. The detailed explaination for EMG phenomena have been study by previous researcher in [9].

Figure 2 shows the abnormal spontaneous activity based on EMG signal. Signal in (figure 2A) shows th fibrillation (*) and positive sharp wave (**) in an acutely denervated hand muscle . Next, signal in (figure 2B) shows the single, doublet, triplet, and multiplet motor unit neuromyotonic discharges is up to 200Hz. While, signal in (figure 2C) shows fasciculations in the tonque in a patient with amyotopic lateral sclerosis.The single discharges are irregular and occur on a background of ongoing EMG activity cause by poor relaxation. Lastly, signal in (figure 2D) shows Myotonic discharges in a patient with dystrophia myotonica. There is a characteristic waxing and waning in frequency [9].

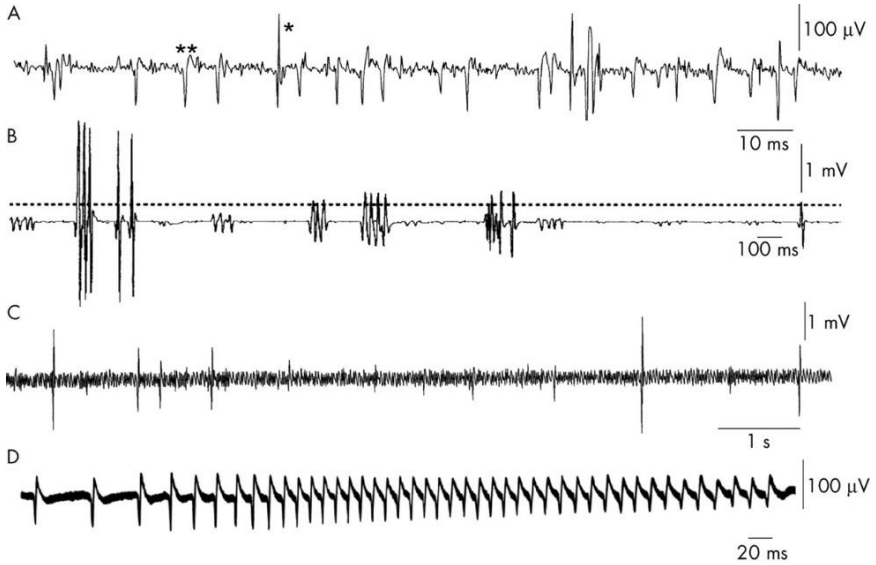

Figure 2 : Abnormal spontaneous activity : (A) Fibrillations , (B) Neuromyotonic, (C) Fasciculations and (D) Myotonic [9]

3.0 MACHINE LEARNING

The name of the psychologist Frank Rosenblatt from Cornell University is typically associated with the origin of Machine Learning (ML) in its modern sense. Rosenblatt was the leader of a group that developed a machine for recognising the letters of the alphabet Rosenblatt. These ideas were based on Rosenblatt's speculations regarding the operation of the human nervous system. (1957, 1959, 1960). The system, which its developer named the "perceptron," utilised both analogue and discrete impulses and had a threshold element that transformed analogue signals to discrete ones [10].

ML is a subset of Artificial Intelligence (AI) that holds that a computer algorithm can learn and adapt to new data without the need for human intervention. ML is an important subfield in Artificial Intelligence (AI). In contrast to the goal of AI, which is to create an intelligent system or assistant using various ML approaches to solve problems, the goal of ML is to create computer systems that can learn and respond based on their prior observation. [11]. Figure 3 shows the relation between AI and ML.

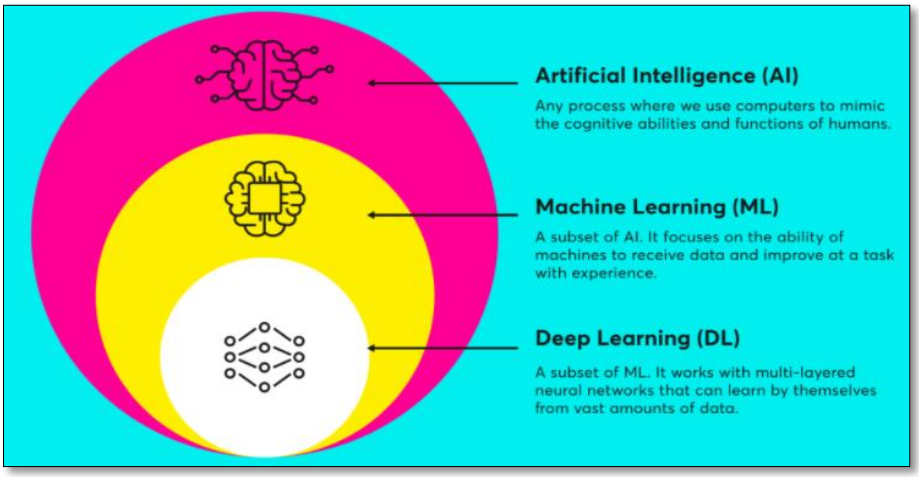

Figure 3 : Relation between Artificial Intellegent (AI) , Machine Learning (ML) and Deep Learning (DL)[12].

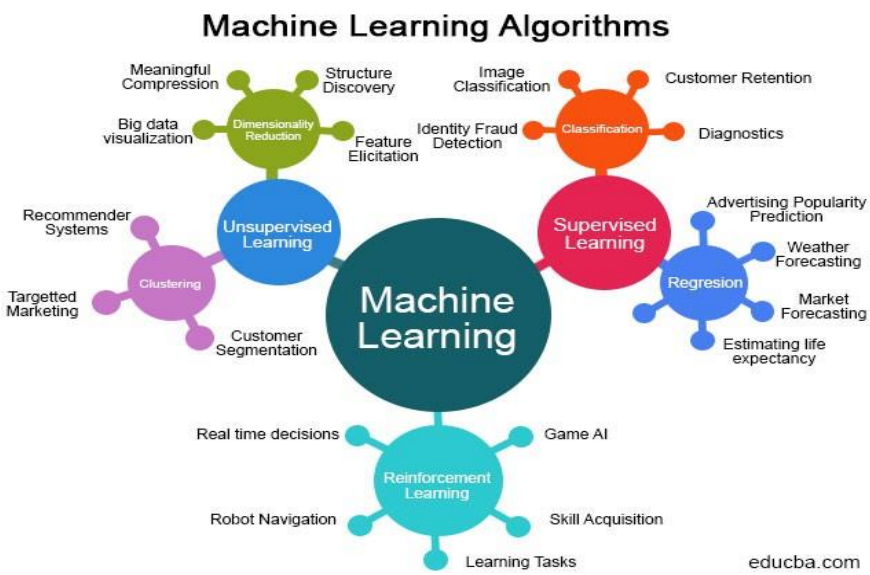

Figure 4 : Types of ML algorithm for data processing [16].

ML methods, are generating a lot of interest in commercials, professionals and academic applications [13] [10] . ML has also been very successful in getting important information out of data for a wide

range of applications. Most of the researchers today agree that there is no intelligent without learning [14]. It reduces costs and the amount of labour needed while simultaneously improving data-oriented analysis and increasing hit ratio. On the other hand, there is still a requirement to investigate the outcomes using a variety of classifiers on a dataset taken from the real world..[15]. Since their inception, ML algorithms have been used to analyse medical datasets. Today, ML offers a variety of vital tools for intelligent data analysis. Figure 4 depicts the data processing ML algorithms.

ML Algorithms vary in their approach, the data they utilise as input and output, and the tasks or problems they are designed to address. Figure 4 shows that ML algorithm can be categorized into supervised learning, unsupervised learning and reinforcement learning. Among those techniques, supervised learning is the most frequently used, which becomes the major focus in this paper. The summary of explanation about ML algorithm have been revealed by [17] as shows in Table 1 below:

Table 1 : Category of ML algoritms

Categorized ML Algorithm	**Summary of Explaination**
Supervised Learning	The various algorithms generate a function that maps inputs to desired outputs. One standard formulation of the supervised learning task is the classification problem: the learner is required to learn (to approximate the behavior of) a function which maps a vector into one of several classes by looking at several input-output examples of the function
Unsupervised Learning	Models a set of inputs: labeled examples are not available
Reinforcement Learning	The algorithm learns a policy of how to act given an observation of the world. Every action has some impact in the environment, and the environment provides feedback that guides the learning algorithm

4.0 TYPES OF MACHINE LEARNING CLASSIFIER

In this subtopic, the details of supervised ML classifier are pointed. Supervised learning which we use an algorithm to learn the mapping function (f(X)) from the input variables (X) so that we can predict the outcome (Y) for the dataset. Supervised learning can be categorize into classification and regression. However, the classification is the most widely used techniques. The processs flow of applying supervised ML is described in Figure 5.

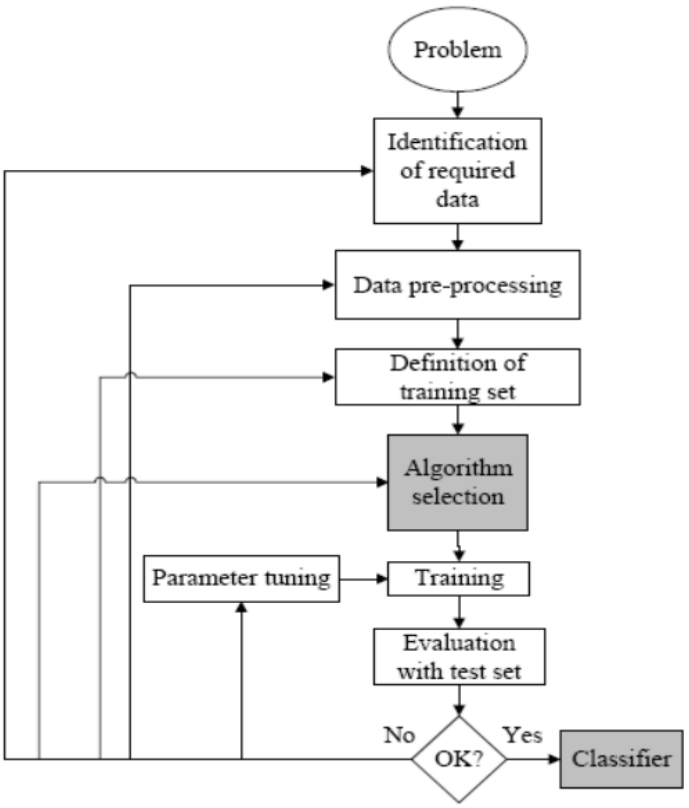

Figure 5 : Supervise ML Process Flow [18]

Types of ML algorithm (classifier) can be used in classification tasks such as k-nearest (KNN), discriminate analysis (DA), naïve Bayes (NB), random forest (RF), decision tree (DT) , logistic regression (LR) , support vector machine (SVM) and Neural Network (NN). There are numerous classification algorithms now available, however it is

impossible to determine which one is preferable. It depends on the application and the type of data set provided.

i. K-nearest-neighbour's (KNN)

KNN is supervised learning method and has a useful and accurate classification [19], [20]. The data represented in KNN method in form of vector space[21]. The Euclidean distance is used to measure the distance between points using the given Eq. (1) [21], [22]:

$$D_i = \sum_k^h \sqrt{(x_i - x_k)^2 + (y_i - y_k)^2} \quad (1)$$

Where k represents a variable and selects as an essential factor while h represents the least distance from the selected point if k is equal to h, which means unselected point.

ii. Linear Discriminant Analysis (LDA)

LDA (linear discriminate analysis) is a well-known ML approach that gives accurate findings, according to [23][24]. This shows that LDA may offer high consistent outcomes for a long-term EMG impact. LDA is also seen as a less troublesome ML method, particularly overtraining. LDA is a statistical algorithm which is not only covering the boundary points but also the different data points lie on the hyperplane. In addition , LDA calculates the parameter of discriminate function from the training data eveluation the boundary sapce in hyperplane among multiple clasess.

In LDA, it is assumed that the feature vector variables to be multivariate normally distributed. Let C_g (g [1,G]) denotes the movement classes: $\bar{f}$ is the feature vector in one analysis window. The idea of discriminant analysis is to classify the observed features to movement class in which the posterior probability $P(C_g \mid \bar{f})$ can be maximized. The posterior probability is the probability of class C_g given the observed feature vector $\bar{f}$ and can be expressed as:

$$P(C_g \mid \bar{f}) = \frac{P(\bar{f} \mid Cg)\, P(Cg)}{P(\bar{f})} \quad (2)$$

Where $P(C_g)$ is the priori possibility, $P(C_g \mid \bar{f})$ is the likelihood, and $P(\bar{f})$ is the possibility of observed feature vector $\bar{f}$.

iii. Naïve Bayes (NB)

According to [25][26], Naive Bayes (NB) is a ML approach that has been used to categorize and diagnose the location and kinds of harmonic

sources. NB is a well-known and trustworthy ML technique that has been widely used in pattern recognition research. In general, NB estimates the probability of data using the Bayes theorem, provided that all characteristics are independent. NB considers the most likely class while assessing the probability of a feature vector. Naive Bayes may also compete with more difficult classifiers and attain success levels, according to (Yaman 2019)(Nazmi et al., no date). The detection capacity of Nave Bayes is degraded because of the relationships between characteristics. NB make use of bayes theorem to estimate the probability of model would be the self detemining feature model. In basic term, a NB classifier asssumes that the presence of a particular feature of a class is unrelated to the presence of any other feature [27].Mathematically, the model posterior probability based on Bayes rule can be represented as:

$$P(Y = k \mid X_1 \ldots, X_p) = \frac{\pi(Y=k) \prod_{j=i}^{p} P(X_j \mid Y=k)}{\sum_{k=1}^{K} \pi(Y=k) \prod_{j=i}^{p} P(X_j \mid Y=k)} \quad (3)$$

Where K is the number of classes, Y is random variable corresponding to class index k of an observation , X is the random predictor of observation, and $\pi(Y = k)$ is the prior probability that a class index is k.

Naturally, NB identifies the most probable class by evaluating the probability of new features.The advantage of the NB classifier is that it only requires a small amount of training data to estimate the means and variances of the variable necessary for classification.Because of independent variablex are unspecified, only the variances for each label need to be determined and not the entire covariance matrix [28]. However, NB is very sensitive to the appearance of noise and redundancy. There are severaly types of distribution that can be used in NB such as normal distribution or Gaussian distribution fo kernel smoothing density prediction.

iv. Support Vector Machine (SVM)

ML approaches such as support vector machines (SVM) are utilized to detect and diagnose the location and kind of harmonic sources, according to (Jopri et al., 2020). SVM is a complex ML technique that has been used in a wide range of applications. By increasing the feature vector size, SVM applies the notion of hyperplane separation to data. According to [23], the support vector machine (SVM) has been

identified as one of the most successful and efficient ML methods in the field of EMG pattern recognition. SVM has lately emerged as a high-potential classifier that outperforms others in terms of accuracy. SVM partitions the data set on the hyperplane using the concept of separation, enabling all data to be divided linearly. Furthermore, SVM is the best classification function for discriminating between classes in a spectrogram feature set since it maps data on a high-dimensional space. On the other hand, SVM has a kernel function selection limitation and a high processing cost.

Furthermore, according to [29][2], both linear and nonlinear data are identified using SVM. SVM translates the primary training set into an upper-level size via a nonlinear mapping. In this increased size, SVM searches for the linear optimal separation hyperplane, a decision border between two classes of tuples. A hyperplane with an appropriate nonlinear mapping to an upper dimension can be employed to split data into two groups. This hyperplane creates support vectors, important training vectors, and margins. In comparison to other procedures, they are particularly resistant to overfitting.

Figure 6 shows the graphical of SVM classifier. It is shown that the two separable classes of observations with the maximum margin separating line (solid) and second separating line (dashed). Blue and red denote the two classes (y values) and denote support vectors[30].

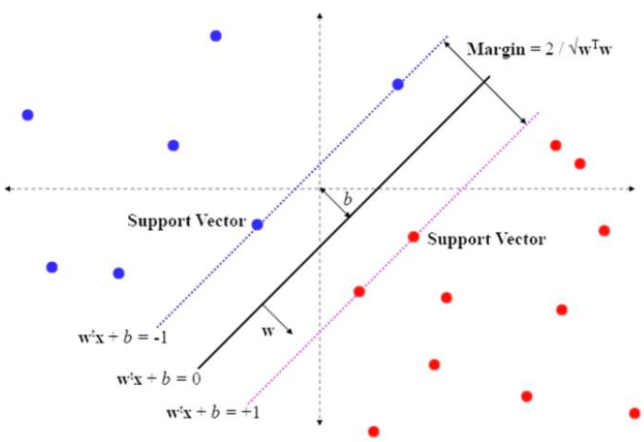

Figure 6 : The graphical SVM classifier [30]

A binary classifier is a function f:X → Y that assigns each point as x ∈ X with some y ∈ Y. Both linear SVM and quadratic SVM use kernel version classifiers as its foundation.

$$f(x) = \sum_i \propto_i y_i \ (x_i^T \ x) + b \tag{4}$$

where w > x + b = 0 and c (w > x + b) = 0 define the same plane [30][31].

The normalization of w for both cases as positive and negative support vectors can be choose. Choose normalization such that:

$$(w_i^T \ x_+) + b = 1 \tag{5}$$
$$(w_i^T \ x_-) + b = 1 \tag{6}$$

The margin is expressed as:

$$\frac{w}{||w||} . (x_+ - \ x_-) = \frac{w^T \ (x_+ - \ x_-)}{||w||} = \frac{2}{||w||} \tag{7}$$

The mathematical formulated of learning SVM algorithm as below:

$Max_w \frac{2}{||w||} \ subject \ to \ w^T \ x_+ + b \quad \geq 1$ if $y_i \ = +1$

≤ 1 if $y_i \ = -1$

For i = 1…N

$\text{Min}||w||^2 \ subject \ to \ y_i \ (w^T \ x_+ + b) \ \geq 1$ for $i = 1 \ldots N$

5.0 APPLICATION OF MACHINE LEARNING METHOD FOR EMG SIGNAL ANALYSIS

Electromyography (EMG) is the study of muscle function by electrical signal analysis during muscular contractions. [32]. The electrodes, which are the electrical sensors, are positioned on the skin directly above the muscles of interest, and the EMG signals provide information regarding the activation of the muscle, the force produced by the muscle, and the state of the muscle. [33] . All of these components are superimposed, meaning that the EMG signal measurement combines the contributions from many sources. Consequently, it is challenging to obtain information about a specific element by examining the EMG signal. Table 2 shows the details research work which describe the ML methods used to analyse the EMG signal. Individual columns healthcare application area, ML algorithm, the data used for the study, and the study results.

Table 2 : Summary of works carried out using ML algorithms with EMG signals

Author	Application	ML Algorithm	Data	Results
[34]	Kinematic and Dynamic Biomechanical Variables	RNN RCNN	17 healthy right-handed (9 Females and 8 Males; performing lifted and lowered a weighted object between two target locations	Complete estimation for biomechanical signal reach accuracy (96.9%)
[30]	Hand Movement classification	QDA, SVM, random forest, ensemble (subspace KNN)	10 healthy subjects (5 males and 5 females) performing 4 gesture movements include stationary, double tap, single finger movement and finger spread	Accuracy of 83.9%
[35]	Smart Terrain Identification for Lower Limb Rehabilitation	SVM	10 healthy subjects (6 males and 4 female) instructed to work at confortable speed (walking habit)	Accuracy of 96.8%
[36]	Finger Movements for Prosthesis Control	ANN	5 healthy subjects (4 males and 1 female) performing 11 finger movements	Recognation accuracy reach (91.10%)
[37]	Ambulation mode for lower limb	SVM	18 participants performing 4 different ambulatory activities	Recognize ambulation task categories with best accuracy (94.29%).
[38]	Hand movement classification	LDA	5 healthy subjects (2 males and 3 females) performing six different hand movement	Accuracy of 97.56%
[39]	Shoulder motion classification	RF	6 upper limb amputee subjects performing rest,	Accuracy of 98%

	for upper limb amputees		elevation,retraction and protraction motion	
[31]	Robust Control of hand prostheses	LDA and SVM (WT/SVM-OVO)	Transradial amputees performing fist, fingers spread, four-finger close, forearm supination, forearm pronation, open, and no motion	Accuracy of 92.3%
[40]	Upper limb phantom movement classification	ANN	5 transhumeral amputees participated performing 8 upper limb phantom movement	Accuracy of 60.9% to 93.0%
[41]	Shoulder Movement Classification	NN and LDA	8 healthy subjects (4 males and 4 female) performing 8 shoulder movements	Accuracy of 92%
[42]	Hand motion classification	LDA, QDA, SVM, ANN, KNN and Random Forest (RF)	8 healthy subjects (3males and 5 female)Three grasping things (mug, marker, rectangle) at three different places to observe	Accuracy of 83%
[43]	Hand movement classification	SVM, naïve bias and KNN	9 subjects walking, running, resting and open door	Accuracy more than 90%

Despite the fact that ML has been utilised for a long time, published studies have proven that it is capable of making faster and more reliable diagnoses in physiological signals.The potency may well trigger a shift way from the current used decision support methods such as SVM and Neural Network (NN), towards ML. Table 2 demonstrates that the application of ML to the analysis of an electromyographic (EMG) signal improved diagnostic accuracy. This is due to the fact that the proposed model successfully extracts unique characteristics from the EMG data. This classifier features allow the network to be trained even without big data, leading to satisfactory diagnostic results. In contrast, the automated analysis of EMG signals

is more difficult due to the chaotic character of these signals. Therefore, it is more difficult for the network to learn from these signals' concealed and delicate information.

In Table 2 also shows the ML algorithm types that has been used by previous researcher works to analyse a EMG signal. Overall, SVM, KNN and LDA are most popular ML algorithm that used in diagnosis of EMG signal especially for upper limbs of our body. Apart from the algorithm, Table 2 also shows the data types used to implement the ML algorithm. SVM, KNN and LDA classifier are the most used for hand movement activity with the best accuracy compare to the other classifiers.

6.0 CONCLUSION

In this paper have been reviewed on the ML methods applied to healthcare application based on Electromyography (EMG) signals. The paper also go through the mathematical formula to decribe the ML algorithms. ML is one of the artificial intelligence that make the decisions to achieve the objective.ML algorithm is useful for identifiying patterns in observed data, build models and predict things without having explicit programmed rules and models. The learning model can be any classifier such as a KNN, LDA, NB and SVM. In this review revealed that SVM, KNN and LDA are most popular ML algorithm that used in diagnosis of EMG signal especially for upper limbs of our body because mostly the accuracy for the respective classifier shows that more than 80 to 90% accurate results.

7.0 ACKNOWLEDGEMENTS

The authors would like to thanks the Universiti Teknikal Malaysia Melaka (UTeM), Faculty of Electrical and Electronic Engineering Technology (FTKEE) and Faculty of Electrical Engineering (FKE), Advance Digital Signal Processing (ADSP) Lab, Centre of Robotic and Industrial Automation (CeRIA) , Motorcycle Engineering Technology Lab (METAL), Faculty of Mechanical Engineering, Universiti Teknologi MARA, 40450 Shah Alam, Selangor, Malaysia and Ministry of Higher Education (MOHE), Malaysia that supported this research under project FRGS/1/2020/FTKEE CERIA/F00428.

8.0 REFERENCES

[1] A. Manca *et al.*, "A Survey on the Use and Barriers of Surface Electromyography in Neurorehabilitation," *Front. Neurol.*, vol. 11, 2020.

[2] D. C. Toledo-Pérez, J. Rodríguez-Reséndiz, R. A. Gómez-Loenzo, and J. C. Jauregui-Correa, "Support Vector Machine-based EMG signal classification techniques: A review," *Appl. Sci. Switz.*, vol. 9, no. 4402, pp. 1–28, 2019.

[3] H. Rashid *et al.*, "Usage of Wireless Myon 320 Surface Electromyography (sEMG) System in Recording Motorcyclist Muscle Activities on Real Roads: A Case Study," *Procedia Manuf.*, vol. 3, no. Ahfe, pp. 2566–2573, 2015.

[4] H. A. Yousif *et al.*, "Assessment of Muscles Fatigue Based on Surface EMG Signals Using Machine Learning and Statistical Approaches: A Review," in *IOP Conference Series: Materials Science and Engineering*, 2019, p. 705(1).

[5] T. N. S. T. Zawawi, A. R. Abdullah, R. Sudirman, N. Saad, and N. H. Mahmood, "A Review of Electromyography Signal Analysis of Fatigue Muscle for Manual Lifting," in *6th International Conference on Computing, Engineering, and Design, ICCED 2020*, 2020.

[6] E. F. Shair, S. A. Ahmad, M. H. Marhaban, S. B. M. Tamrin, and A. R. Abdullah, "EMG processing based measures of fatigue assessment during manual lifting," *BioMed Res. Int.*, vol. 2017, pp. 1–12, 2017.

[7] D. Nam, J. M. Cha, and K. Park, "Next-generation wearable biosensors developed with flexible bio-chips," *Micromachines*, vol. 12, no. 1, p. 64, 2021.

[8] M. Kazamel and P. P. Warren, "History of electromyography and nerve conduction studies: A tribute to the founding fathers," *J. Clin. Neurosci.*, vol. 43, pp. 54–60, 2017.

[9] K. R. Mills, "The basics of electromyography," *Neurol. Pract.*, 2005.

[10] A. L. Fradkov, "Early history of machine learning," in *IFAC-PapersOnLine*, 2020, pp. 1385–1390.

[11] J. Chaki, S. Thillai Ganesh, S. K. Cidham, and S. Ananda Theertan, "Machine learning and artificial intelligence based Diabetes Mellitus detection and self-management: A systematic review," *J. King Saud Univ. - Comput. Inf. Sci.*, 2020.

[12] Samantha Wolhuter, "Demystifying AI Part 6: Machine Learning vs Deep Learning — what's the difference?," May 25, 2019. https://wearebrain.com/blog/software-development/machine-learning-vs-deep-learning/ (accessed Feb. 28, 2022).

[13] R. Roscher, B. Bohn, M. F. Duarte, and J. Garcke, "Explainable Machine Learning for Scientific Insights and Discoveries," *IEEE Access*, vol. 8, pp. 42200–42216, 2020.

[14] I. Kononenko, "Machine learning for medical diagnosis: History, state of the

art and perspective," *Artif. Intell. Med.*, vol. 23, no. 1, pp. 89–109, 2001.

[15] K. M. Ghori, R. A. Abbasi, M. Awais, M. Imran, A. Ullah, and L. Szathmary, "Performance Analysis of Different Types of Machine Learning Classifiers for Non-Technical Loss Detection," *IEEE Access*, vol. 8, pp. 16033–16048, 2020.

[16] D. Aggarwal, "Image Segmentation Techniques using Digital Image Processing, Machine Learning and Deep Learning Methods. (Part 2) | by Deeksha Aggarwal | Analytics Vidhya | Medium," 2020. https://medium.com/analytics-vidhya/image-segmentation-techniques-using-digital-image-processing-machine-learning-and-deep-learning-ccf9e4589e94 (accessed Mar. 01, 2022).

[17] V. Nasteski, "An overview of the supervised machine learning methods," *HORIZONS.B*, vol. 4, pp. 51–62, 2017.

[18] O. F.Y, A. J.E.T, A. O, H. J. O, O. O, and A. J, "Supervised Machine Learning Algorithms: Classification and Comparison," *Int. J. Comput. Trends Technol.*, vol. 48, no. 3, pp. 128–138, 2017.

[19] G. Guo, H. Wang, D. Bell, Y. Bi, and K. Greer, "KNN model-based approach in classification," *Lect. Notes Comput. Sci. Subser. Lect. Notes Artif. Intell. Lect. Notes Bioinforma.*, vol. 2888, pp. 986–996, 2003.

[20] L. Chen, M. Li, W. Su, M. Wu, K. Hirota, and W. Pedrycz, "Adaptive feature selection-based AdaBoost-KNN with direct optimization for dynamic emotion recognition in human-robot interaction," *IEEE Trans. Emerg. Top. Comput. Intell.*, vol. 5, no. 2, pp. 205–213, 2021.

[21] N. T. Mahmood, M. H. Al-Muifraje, and S. K. Salih, "EMG Signals Classification of Wide Range Motion Signals for Prosthetic Hand Control," *Int. J. Intell. Eng. Syst.*, vol. 14, no. 5, pp. 410–421, 2021.

[22] M. Z. Jahromi, E. Parvinnia, and R. John, "A method of learning weighted similarity function to improve the performance of nearest neighbor," *Inf. Sci.*, vol. 179, no. 17, pp. 2964–2973, 2009.

[23] J. Too, A. R. Abdullah, N. M. Saad, N. M. Ali, and T. N. S. T. Zawawi, "Classification of myoelectric signal using spectrogram based window selection," *Int. J. Integr. Eng.*, vol. 11, no. 4, pp. 192–199, 2019.

[24] S. Young, B. Stephens-Fripp, A. Gillett, H. Zhou, and G. Alici, "Pattern recognition for prosthetic hand user's intentions using EMG data and machine learning techniques," in *IEEE/ASME International Conference on Advanced Intelligent Mechatronics, AIM*, 2019, pp. 544–550.

[25] M. H. Jopri, A. R. Abdullah, J. Too, T. Sutikno, S. Nikolovski, and M. Manap, "Support-vector machine and Naïve Bayes based diagnostic analytic of harmonic source identification," *Indones. J. Electr. Eng. Comput. Sci.*, vol. 20, no. 1, pp. 1–8, 2020.

[26] B. Karlık, "Machine Learning Algorithms for Characterization of EMG Signals," *Int. J. Inf. Electron. Eng.*, vol. 4, no. 3, 2014.

[27] Y. Ma, S. Liang, X. Chen, and C. Jia, "The approach to detect abnormal access behavior based on naive bayes algorithm," in *Proceedings - 2016 10th International Conference on Innovative Mobile and Internet Services in Ubiquitous Computing, IMIS 2016*, 2016, pp. 313–315.

[28] W. Feng, J. Sun, L. Zhang, C. Cao, and Q. Yang, "A support vector machine based naive Bayes algorithm for spam filtering," in *2016 IEEE 35th International Performance Computing and Communications Conference, IPCCC 2016*, 2017, pp. 1–8. doi: 10.1109/PCCC.2016.7820655.

[29] E. Yaman and A. Subasi, "Comparison of Bagging and Boosting Ensemble Machine Learning Methods for Automated EMG Signal Classification," *BioMed Res. Int.*, vol. 2019, pp. 1–13, 2019.

[30] H. A. Javaid *et al.*, "Classification of hand movements using myo armband on an embedded platform," *Electron. Switz.*, vol. 10, no. 11, 2021.

[31] A. Nastarin, A. Akter, and M. A. Awal, "Robust control of hand prostheses from surface EMG signal for transradial amputees," in *2019 5th International Conference on Advances in Electrical Engineering, ICAEE 2019*, 2019, pp. 143–148.

[32] "Electromyography: Fundamentals," in *International Encyclopedia of Ergonomics and Human Factors - 3 Volume Set*, 2021, pp. 3155–3162.

[33] O. Faust, Y. Hagiwara, T. J. Hong, O. S. Lih, and U. R. Acharya, "Deep learning for healthcare applications based on physiological signals: A review," *Comput. Methods Programs Biomed.*, vol. 161, pp. 1–13, 2018.

[34] A. Nasr *et al.*, "MuscleNET: Mapping electromyography to kinematic and dynamic biomechanical variables by machine learning," *J. Neural Eng.*, vol. 18, no. 4, 2021.

[35] S. Gao, Y. Wang, C. Fang, and L. Xu, "A smart terrain identification technique based on electromyography, ground reaction force, and machine learning for lower limb rehabilitation," *Appl. Sci. Switz.*, vol. 10, no. 8, 2020.

[36] Z. Zhang, X. Yu, and J. Qian, "Classification of finger movements for prosthesis control with surface electromyography," *Sens. Mater.*, vol. 32, no. 4, pp. 1523–1532, 2020.

[37] B. Zhou *et al.*, "Accurate recognition of lower limb ambulation mode based on surface electromyography and motion data using machine learning," *Comput. Methods Programs Biomed.*, vol. 193, 2020.

[38] J. Too, A. R. Abdullah, and N. M. Saad, "Classification of Hand movements based on discrete wavelet transform and enhanced feature extraction," *Int. J. Adv. Comput. Sci. Appl.*, vol. 10, no. 6, pp. 83–89, 2019.

[39] K. Amanpreet, "Machine learning-based novel approach to classify the

shoulder motion of upper limb amputees," *Biocybern. Biomed. Eng.*, vol. 39, no. 3, pp. 857–867, 2019.

[40] G. Gaudet, M. Raison, and S. Achiche, "Classification of Upper limb phantom movements in transhumeral amputees using electromyographic and kinematic features," *Eng. Appl. Artif. Intell.*, vol. 68, pp. 153–164, 2018.

[41] D. Rivela, A. Scannella, E. E. Pavan, C. A. Frigo, P. Belluco, and G. Gini, "Analysis and Comparison of Features and Algorithms to Classify Shoulder Movements from sEMG Signals," *IEEE Sens. J.*, vol. 18, no. 9, pp. 3714–3721, 2018.

[42] I. Mendez *et al.*, "Evaluation of the Myo armband for the classification of hand motions," in *IEEE International Conference on Rehabilitation Robotics*, Aug. 2017, pp. 1211–1214.

[43] S. Pizzolato, L. Tagliapietra, M. Cognolato, M. Reggiani, H. Müller, and M. Atzori, "Comparison of six electromyography acquisition setups on hand movement classification tasks," *PLoS ONE*, vol. 12, no. 10, pp. 1–17, Oct. 2017.

RECENT ADVANCES IN COMPUTED TOMOGRAPHY RADIATION DOSIMETRY

H. G. Sarhan[1*], N. M. Noor[1,2*], S. M. Saini[1,2] and N. M. Bahari[1,2]

[1]Medical Physics Laboratory, Faculty of Medicine and Health Sciences, Universiti Putra Malaysia, 43400, Serdang, Selangor, Malaysia.

[2]Department of Radiology, Teaching Hospital Universiti Putra Malaysia, 43400, Serdang Selangor.

[*]Corresponding Author's Email: gs54005@student.upm.edu.my; noramaliza@upm.edu.my

Article History: Received January 17, 2023; Revised January 26, 2023; Accepted January 26, 2023

ABSTRACT: Computer tomography (CT) has proved fundamental in image evaluation throughout the past three decades. By combining rapid scanning with high-quality data sets, multi-detector technology continues to influence practice patterns. This has led to new applications and improved use in conventional applications. However, the increased use of CT has generated significant concern regarding the high radiation doses received by patients during CT scans compared to traditional radiography examinations. Many studies have been undertaken on minimizing patient dose and adhering to the as low as reasonably achievable (ALARA) principle. A total of 40 articles from PubMed, Science Direct and Google Scholar were systematically summarized in this review paper to introduce the growth of CT scan from single-slice to multi-slice technology from 2000 until December 2020 as well as dual-energy and multi-detector CT technologies. The important role of utilizing CT radiation dosimeters for CT dose measurement is defined included CT dose reduction techniques.

KEYWORDS: *CT dose reduction techniques; CT radiation dosimetry; Dual-energy CT; Multi-detector CT; Multi-slice CT*

1.0 INTRODUCTION

1.1 CT Generation from Single-Slice to Multi-Slice Scanner

CT scans have been in clinical use for about 30 years, and they are now used in almost every hospital environment. CT imaging technology has advanced from scanning a single slice to spiral CT, and then to a multi-slice scanner. In the first conventional CT scanners, the tube and a row of detectors are located on opposing sides of a spinning ring around the patient. Since the tube is connected to the power cables, it cannot rotate continuously. The scanner stops and rotates in the opposite direction after each rotation. It takes one rotation to acquire an axial image, with a thickness of 1 cm, and the process takes about one second per rotation [1]. The movement of the patient through the scanner is made by moving the table between each slice. Hence, there are some drawbacks to conventional scanners, scan time is long to run, and this results in noise due to movement or breathing. In addition, scanners have an irregular ability to reformat in different planes, dynamic contrast analyses are also extremely difficult, and even small tumors can be missed between slices [2].

Since conventional CT scanners are considered as time-consuming. Hence, great efforts were made in the late 1980s to increase scanning volumes in less time [3]. This concept led to the creation of a new technique that was utilized by moving the table while the x-ray tube and detectors rotate for several times to perform scans of tissue. As a result, the beam travels in a circle around the patient. This is technically known as spiral CT, however others refer to it as helical CT [4]. In 1998, the introduction of a new generation of CT scanners was made at the Radiological Society of North America (RSNA) meeting in Chicago [5]. These scanners are known as multislice CT (MSCT) scanners. Multislice CT was developed by adapting single-slice CT (stop-and-go, slice-by-slice data acquisition), which was more flexible in dealing with the limitations of conventional CT. In doing so, multislice CT scanners could reduce the time for data acquisition, thus speeding up the volume coverage. A "turbocharged" spiral scanner is another name for a MSCT scanner [6]. The single row of detectors used by spiral and conventional scanners to detect the x-ray beam once it has passed through the patient. On the other hand, up to eight active detector rows can be used with a multi-slice scanner. Coverage of a given volume of tissue is increased because of the increased detector and tube rotation times that take less than a second to complete [7], [8]. In newer multi-slice scanners, faster computer software is also included, making the processing of reconstructed images and post-processing faster. A multi-slice scanner with four detectors theoretically will reduce scan time by a quarter compared to a single slice spiral scanner [1], [2].

Multi-slice scanners have the ability to scan images two to three times faster than single-slice scanners in practice. As seen in Figure 1, the number of slices each revolution has increased steadily over time.

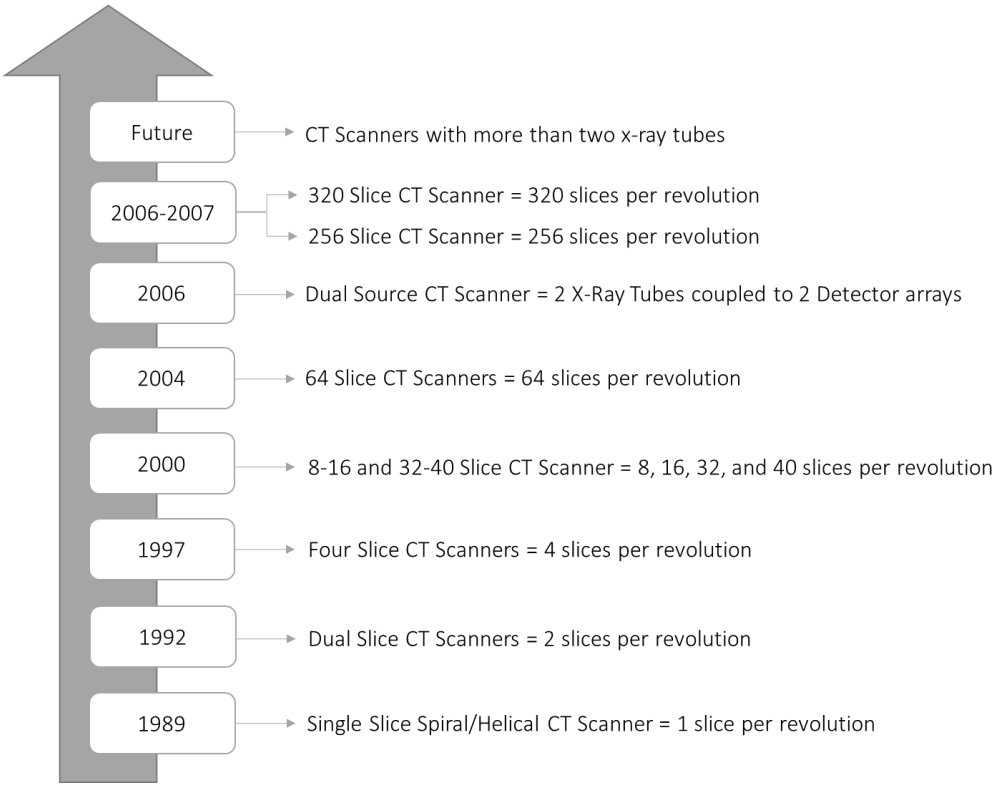

Figure.1 The evolution of MSCT scanners, including the DSCT scanner [2]

1.2 Overview of Multi-detector CT Technology

There have been considerable developments in computer tomography technologies in recent years such as cone beam, extreme multi-detector, dual-energy, portable, and phase contrast in CT technology. The primary difference between single-slice CTs and multi-slice CTs is a technology for detectors. The "multi-detector-row" type of MDCT scanners refers to multiple arrays (rows) in the z-direction [9]. Now available MDCT scanning systems utilize CT geometry of the third generation, which rotates the range of detectors together with the x-ray tube(s). Due to their improvements, these scanners offer enormous versatility not only in detector technology, but also in the data acquisition systems (DAS), X-ray tubes, and other subsystems. One

example is that whereas MDCT scanners feature multiple rows of detectors, the collected data from multiple rows of detectors can be merged as if collected from one single detector [10], [11].

One of the most significant components of the CT imaging chain is the detector because it detects radiation transmitted by the body and transforms it into electrical signals that are then digitized and forwarded to the computer for processing and image creation. Currently, two types of detectors detect and transfer radiation into digital data [12]. Scintillation and photon-counting are examples of these detectors [13]. Figure 2 illustrates the major components of two types of scintillation detectors: traditional energy integrating and dual-layer. Scintillation crystals in the MSCT include cadmium tungstate (CdWO4); high purity ceramic material, rare earth oxides, based on rare-earth-doped compounds as yttria; and gadolinium oxysulfide ultrafast ceramic. GE Healthcare has implemented gemstone spectral imaging, the world's first garnet scintillator for use in computed tomography. Additionally, Philips Healthcare also utilizes zinc selenide triggered with tellurium in their dual-layer scintillator detectors [14]. The photon-counting detector is a new technology that is being investigated in prototype scanners such as Siemens SOMATOM Definition Flash [15]. Semiconductors such as cadmium telluride (CdTe) and cadmium zinc telluride (CZT) are used because they can immediately convert x-ray photons into pairs of electron-hole (electric charge).

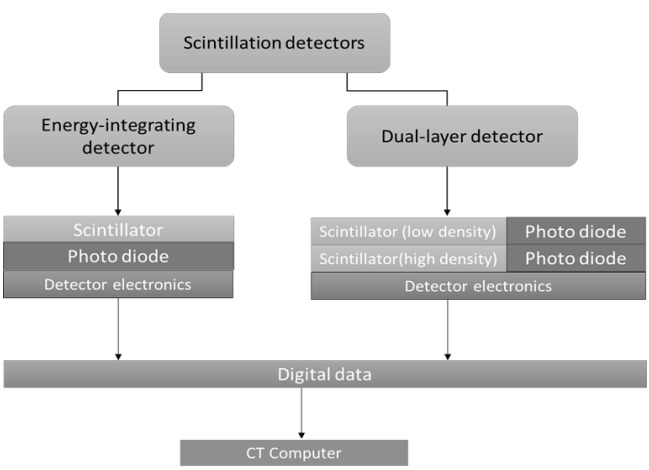

Figure 2. The main components of two types of scintillation detectors [12, 13,14, 15]

1.3 Dual-Energy Computed Tomography

Advancements in multidetector technology have made imaging possible for dual-energy computed tomography (CT). In 2006, a CT scanner was presented at the RSNA meeting mainly for cardiac imaging and other applications [16]. The latest improvements in multidetector CT (MDCT) capabilities include two-source and single-source designs, allow almost simultaneous image acquisition at mainly two kVps for dual-energy imaging, allowing the study of different tissue and material components inside a CT image's voxels [3]. The existing dual-energy CT system utilizes a higher kVp of 140 (labeled A) and a lower one of either 80 or 100 kVp (labeled B), each tube has a corresponding detector positioned on a rotating gantry opposite the tube. The radiation beams of the 2 tubes are parallel to each other at a 90-degree angle at the isocentre. The A tube has been associated with a maximum field of view (FOV) of 50 cm because of its detector size while the B tube has a maximum FOV of 26 cm in the first generation of the dual-source MDCT scanner.

CT imaging of the heart using MSCT scanners began in 1999, and due to the constant motion of the heart (heartbeat), temporal resolution is critical to avoid motion artifacts [17]. Additionally, it is critical to cover the entire heart with a single breath-hold when performing cardiac imaging with CT. Despite four-slice CT scanners have offered satisfactory results, issues with long breath-holding, artifacts motion, higher heart rates, and poor spatial resolution still persisted [18].

One of the issues with CT cardiac imaging is the elimination of the necessity for cardiac rate control, hence efforts are necessary to increase time resolution below 100 ms at any heart rate. Other scanners are needed to solve these issues, such as the electron beam CT. While this scanner has some advantages in imaging, it does not offer an acceptable signal-to-noise ratio in large patients. This scanner is therefore not currently deemed suitable for state-of-the-art cardiac CT imaging. To further increase the time resolution required by a factor of two another CT scanner for cardiac CT imaging, the DSCT scanner for cardiac imaging (developed by Siemens Medical Solutions), was termed the definition [14].

This review paper presents the history of CT scanner in terms of CT generations from single-slice to multi-slice scanners, with emphasis on the development of Multi-detector CT technology. The second section of this paper focus on the current different types of CT radiation

dosimeters used for CT dose measurement including the pros and drawbacks of each CT radiation dosimeter. Besides, this article also reviews the CT radiation dose to patients and outlines the certain units and terminology that are relevant to the CT, and strategies for minimizing CT radiation dose.

2.0 METHODOLOGY

2.1 CT RADIATION DOSIMETRY

Several types of CT radiation dosimeters have been used previously for dose measurement in CT. These include standard ionization chambers, solid-state semiconductor detectors, radiographic film dosimeters, and thermoluminescent dosimeters (TLDs). In 1981, the Center for Devices and Radiological Health (CDRH) introduced the important step towards measuring the CT dose [19].

Conventional ionization chambers cannot be used to measure the absorbed dose as large beamwidths in CT scanners with multiple beam apertures are present. When a typical CT chamber (10cm) is used to determine the absorbed dose improperly, the dose profile for wide beams is likely to be underestimated [20], [21]. These patient dose problems can be easily addressed with a solid-state dosimetry CT dose profiler made by RTI Group Electronic, Sweden. However, to choose the sort of ionization chamber appropriate to measure CT exposure, two approaches must be considered. The first method is to use a very small volume ionization chamber and to measure a cross-section similar to that used in the TLD measurement [22]. This method has two significant drawbacks: it requires a large number of scans to produce a dose profile and the poor sensitivity of a small volume ionization chamber. The second method involves the use of a long pencil chamber to determine the cross-section of the x-ray field. On the other hand, a RaySafe X2 CT sensor (Unfors RaySafe, Billdal, Sweden) which can be considered as an ionization chamber has been used by many researchers [23].

This type of sensor has been proven to be a successful tool for determining the CT dose. It may be simply inserted into a head/body CT phantom or placed free-in-air. Pressure and temperature are not regulated manually because the sensor contains a method for correctly managing these two factors [5]. However, unlike other dosimeters, the RaySafe X2 CT sensor has the drawback of being unable to identify the CT dose profile [24]. In this situation, the radiographic film is typically

utilized to determine the CT dose profile. Some advantages of the film include inexpensive cost, dose profile indication, reasonably quick working, and availability. Certain disadvantages of the film are qualitative measures, limited dynamic range, densitometry, and limited surface measuring use only [9]. To sum up, the features of an ionization chamber are its high sensitivity and dynamic range, quantitative measurement capabilities, the ability to detect both internal and external exposures, and immediate results. The disadvantages of an ionization chamber are that there is not enough information about the beam profile and the need for a particular chamber because of the X-ray field configuration [25].

Where CTDI is determined by utilizing a CT dose profile probe, the traditional five axial scans are replaced with a single helical scan within the central hole of the phantom. The CT dose profiler has replaced the conventional TLD and OSL methods or radiographic films for measuring the dose profile [26]. The CT dose profiler was designed to be used with a computer system with the Ocean Professional 2014 software. Besides, a narrow beamwidth (<10 mm) is used, the scattering dose of radiation is high beyond 100 mm. [27] studied the scattering index of CT dose when various input parameters were used. The scatter index values were found to be significantly affected by the size of the CTDI phantom and just minimally affected by the voltage applied [27], [28].

Thermoluminescence and semiconductor detector dosimeters are considered in this section. TLDs are available in a variety of forms (powder, chips, rods, and ribbons) and are composed of a variety of materials. While lithium fluoride doped with magnesium and titanium (LiF:Mg,Ti) is the most often used material in medical applications, additional materials such as LiF:Mg,Cu,P; Li2B4O7:Mn; CaSO4:Dy, and CaF2:Mn have also been utilized [28]. High sensitivity and dynamic range, quantitative measurement are the benefits of TLD as well as can be used to measure dose profile. The drawbacks of TLD are the need for an external system for heat stimulation, consuming the time for readout process, and high cost [29]. Certain clinical applications require solid-state semiconductor detectors.

The diode is the basic semiconducting detector, as it is based on a p–n junction between the semiconductor's p- and n-type components. Semiconductor dosimeters enable practical real-time measurements;

the small size of thermoluminescence dosimeters (TLDs) enables their use in patient measurements. Generally, the main limitation of these detectors has been their response energy dependence, which is significantly different from that of ionization chambers. These dosimeters have a variety of purposes, including postal audits and routine clinical assessments in hospitals [30]. The following Table 1.0 shows the comparison between CT radiation dosimetry systems.

Table 1. The comparison between CT radiation dosimeters [9], [20], [21], [24], [29], [30]

CT Radiation Dosimeter	Dosimetry Type	Principle of Operation	Limitation
Conventional Ionization Chamber	Real-time	Ion chamber	1- Cannot be used to measure the absorbed dose as large beamwidths in CT scanners with multiple beam apertures 2- Requires a large number of scans to produce a dose profile and the poor sensitivity of a small volume ionization chamber
CT Sensor from RaySafe X2	Real-time	Ion chamber	1- Unable to measure the width of CT dose profile
Radiographic Film	Passive	Radiophotoluminescence (RPL)	1- Qualitative measures 2- Limited dynamic range 3- Densitometry, and limited surface measuring use only
CT Dose Profile from Black Piranha	Real-time	Solid-state / Semiconductor	1- Ocean Professional Software License required more cost
Thermoluminescence Dosimeters	Passive	Thermoluminescence (TL)	1- Data erased during readout 2- Easy to lose reading 3- Accurate results require care 4- Readout and calibration time consuming

3.0 RESULTS AND DISCUSSION

3.1 CT RADIATION DOSE

CT scans are used in the medical industry, with several CT scans increasing from 3 million in 1980 to 62 million in 2007, alone in the USA. In 1992, the National Radiological Protection Board indicated patients with inappropriate examinations using computed tomography the possibility for high doses [31]. However, the fact that the patient is exposed to radiation by performing CT scans cannot be ignored. Research in the United States in 2009 showed that 75.4% of effective radiation doses from CT scans are around 7 times higher than X-rays. Lately, the CT was utilized in China to diagnose the discovered patient with the coronavirus because of the COVID-19 epidemic and it has been stated that the CT is highly sensitive and needs additional studies carefully [9].

It is necessary to understand certain units and terminology that are relevant to the CT include absorbed dose, effective dose equivalent, and CT dose index (CTDI), and dose length product (DLP) [11]. The absorbed dose is the actual concentration of the radiation dose to a certain organ or tissue measured in Grey (Gy).

The effective dose equivalent enables the conversion of a localized dose to a whole-body equivalent in terms of radiation consequences such as cancer risk. The effective dose equivalent can be calculated mathematically or using anthropomorphic phantoms, or utilizing CTDI or DLP and conversion factors [12], [13].

The CT dose index is measured in a single slice using cylindrical acrylic phantoms of a standard length. For the weighted CTDI (CTDI-w), dosimeters are inserted in the phantom center and periphery holes and the sum of them (weighted dose) is expressed in mGy [8], [31]. This value does not accurately represent the dose contribution of all parameters in helical scanning. For some of this contribution, the volume CTDI or CTDI-vol has lately become more acceptable and considers the contribution from the pitch to CTDI-w. The higher the pitch, the lower the CTDI-vol if all other parameters are constant. The dose length product in a unit (mGy.cm), is calculated as the product of CTDI and scan length, and hence increases proportionally with scan distance covered [1].

3.2 CT DOSE OPTIMIZATION

CT scanner design and performance advancements have contributed to the increased usage of CT in clinical medicine. Numerous studies indicate that CT delivers greater doses to patients than other modalities [32]. For instance, CT doses to individual organs within the image field generally range between 5 and 50 mGy. As of 2011, CT accounted for the most cumulative quantity of medical radiation exposure in the United States, exceeding all other imaging modalities [33]. Paediatric CT examinations with high doses have drawn attention to the cancer risks involved with CT scanning. There has been an increased emphasis on minimizing the dose to the patient without reducing the image quality required for diagnosis [9], [31], [34]. The International Commission on Radiation Protection (ICRP) defines optimization as reducing radiation doses "as low as reasonably achievable" (ALARA) without affecting an image's diagnostic quality. Hence, optimization

considers both radiation dose and image quality.

Several parameters are affecting the dose of the CT patient. These include the scan parameters such as exposure technique factors (mAs and kVp), patient cantering, automatic tube current modulation, collimation, pitch, number of detectors, over-ranging, and iterative image reconstruction [35]. To lower the dose successfully and achieve the required image quality, users need to have systematic procedures or techniques to optimize CT dose. Several researchers have reported different ways of dose optimization in CT, particularly in multi-slice CT [36]–[38]. [31] reviewed optimizing the CT dose and summarised the important items to be considered.

Dose optimization in paediatric CT has gained increasing attention. For instance, [39], [40] provided great overviews on this subject, not only analysing trends and patterns of CT use, CT radiation issues, and how radiologists might control CT dose. They also concentrated on technical aspects of dose management, such as the adjustment of tube current and voltage, the impact of gantry cycle time, and the selection of pitch and detector width. [39] highlighted the significance of the radiologists to confirm that all requested examinations are justified and to ensure that communication is essential as a first step to the reduction of the CT dose between the requesting physicians and radiologists. In addition, an important study in CT pulmonary angiography has shown that the patient's dose is substantially decreased by changing the peak kilovoltage from 120 kVp to 100 kVp with no loss of objective or subjective quality of the image [17].

4.0 CONCLUSION

This review article presented an overview of CT generations from single-slice to multi-slice scanners, with emphasis on the development of Multi-detector CT technology. Many previous research papers are summarised in this review article and mainly focused on the various types of CT radiation dosimeters for CT dose measurement including the advantages and disadvantages of each CT radiation dosimeter. Furthermore, this article reviews the subject of CT radiation dose to patients and outlined the certain units and terminology that are relevant to the CT, and strategies for minimizing CT radiation dose.

5.0 ACKNOWLEDGMENT

The author extends his appreciation to the Medical Physics Laboratory,

Faculty of Medicine and Health Sciences, Universiti Putra Malaysia for supporting this review paper.

6.0 REFERENCES

[1] C. J. Garvey and R. Hanlon, "Computed tomography in clinical practice," *Br. Med. J.*, vol. 324, no. 7345, pp. 1077–1080, 2002, doi: 10.1136/bmj.324.7345.1077.

[2] Z. T. Al-Sharify, T. A. Al-Sharify, N. T. Al-Sharify, and H. Y. Naser, "A critical review on medical imaging techniques (CT and PET scans) in the medical field," *IOP Conf. Ser. Mater. Sci. Eng.*, vol. 870, no. 1, pp. 0–10, 2020, doi: 10.1088/1757-899X/870/1/012043.

[3] D. T. Ginat and R. Gupta, "Advances in computed tomography imaging technology," *Annu. Rev. Biomed. Eng.*, vol. 16, pp. 431–453, 2014, doi: 10.1146/annurev-bioeng-121813-113601.

[4] J. P. Ko, S. Brandman, J. Stember, and D. P. Naidich, "Dual-energy computed tomography: Concepts, performance, and thoracic applications," *J. Thorac. Imaging*, vol. 27, no. 1, pp. 7–22, 2012, doi: 10.1097/RTI.0b013e31823fe0e9.

[5] W. Huda, E. L. Nickoloff, and J. M. Boone, "Overview of patient dosimetry in diagnostic radiology in the USA for the past," *Med. Phys.*, vol. 35, no. 12, pp. 5713–5728, 2008.

[6] S. P. Power, F. Moloney, M. Twomey, K. James, O. J. O'Connor, and M. M. Maher, "Computed tomography and patient risk: Facts, perceptions and uncertainties," *World J. Radiol.*, vol. 8, no. 12, p. 902, 2016, doi: 10.4329/wjr.v8.i12.902.

[7] V. Bertolini *et al.*, "CT protocol optimisation in PET/CT: a systematic review," *EJNMMI Phys.*, vol. 7, no. 1, 2020, doi: 10.1186/s40658-020-00287-x.

[8] L. W. Goldman, "Principles of CT and CT technology," *J. Nucl. Med. Technol.*, vol. 35, no. 3, pp. 115–128, 2007, doi: 10.2967/jnmt.107.042978.

[9] C. McCollough *et al.*, "The Measurement, Reporting, and Management of Radiation Dose in CT," Jan. 2008. doi: 10.37206/97.

[10] D. Dowsett, P. A. Kenny, and R. E. Johnston, *The Physics of Diagnostic Imaging*. CRC Press, 2006.

[11] M. Kachelriess, "Clinical X-Ray Computed Tomography," *New Technol. Radiat. Oncol.*, pp. 41–80, 2006, doi: 10.1007/3-540-29999-8_7.

[12] G. Kohl, "The evolution and state-of-the-art principles of multislice computed tomography," *Proc. Am. Thorac. Soc.*, vol. 2, no. 6, pp. 470–476, 2005, doi: 10.1513/pats.200508-086DS.

[13] E. Seeram, "Computed Tomography: A Technical Review," *Radiol. Technol.*,

vol. 89, no. 3, p. 279CT—302CT, Jan. 2018, [Online]. Available: http://europepmc.org/abstract/MED/29298954.

[14] D. D. Cody and M. Mahesh, "Technologic advances in multidetector CT with a focus on cardiac imaging," *Radiographics*, vol. 27, no. 6, pp. 1829–1837, 2007.

[15] E. Seeram, *COMPUTED TOMOGRAPHY Physical Principles, Clinical Applications, and Quality Control FOURTH EDITION*. 2016.

[16] R. A. Powsner, M. R. Palmer, and E. R. Powsner, *Essentials of Nuclear Medicine Physics and Instrumentation: Third Edition*. 2013.

[17] C. M. Heyer, P. S. Mohr, S. P. Lemburg, S. A. Peters, and V. Nicolas, "Image quality and radiation exposure at pulmonary CT angiography with 100-or 120-kVp protocol: prospective randomized study," *Radiology*, vol. 245, no. 2, pp. 577–583, 2007.

[18] T. G. Flohr *et al.*, "First performance evaluation of a dual-source CT (DSCT) system," *Eur. Radiol.*, vol. 16, no. 2, pp. 256–268, 2006, doi: 10.1007/s00330-005-2919-2.

[19] R. A. Jucius and G. X. Kambic, "Radiation dosimetry in computed tomography (CT)," in *Application of Optical Instrumentation in Medicine VI*, 1977, vol. 127, pp. 286–295.

[20] I. A. Tsalafoutas, M. H. Kharita, H. Al-Naemi, and M. K. Kalra, "Radiation dose monitoring in computed tomography: Status, options and limitations," *Phys. Medica*, vol. 79, pp. 1–15, 2020.

[21] E. C. Corona, I.-B. García Ferreira, J. García Herrera, S. Román López, and O. Salmerón Covarrubias, "Verification of CTDI and DLP values for a head tomography reported by the manufacturers of the CT scanners, using a CT dose profiler probe, a head phantom and a piranha electrometer," *15th Int. Symp. Solid State Dosim.*, pp. 426–435, 2015.

[22] R. A. Powsner, M. R. Palmer, and E. R. Powsner, *Essentials of nuclear medicine physics and instrumentation*. John Wiley & Sons, 2013.

[23] R. Small, P. P. Surujpaul, and S. Chakraborty, "Patient Dose Audit in Computed Tomography at Cancer Institute of Guyana Journal of Medical Diagnostic Methods," vol. 8, no. 1, pp. 1–13, 2019, doi: 10.4172/2168-9784.1000282.

[24] D. J. Brenner *et al.*, "Cancer risks attributable to low doses of ionizing radiation: assessing what we really know," *Proc. Natl. Acad. Sci.*, vol. 100, no. 24, pp. 13761–13766, 2003.

[25] J. M. Boone *et al.*, "4. Overview of Existing CT-Dosimetry Methods," *J. ICRU*, vol. 12, no. 1, pp. 35–45, 2012, doi: 10.1093/jicru/nds004.

[26] B. Cederquist, M. Båth, and J. Hansson, "Evaluation of two thin CT dose profile detectors and a new way to perform QA in a CTDI head phantom," *Dep. Radiat. Physics, …*, 2008, [Online]. Available:

https://www.radfys.gu.se/digitalAssets/1044/1044932_Bj__rn_Cederquist.pdf.

[27] C. Anam *et al.*, "Scatter index measurement using a CT dose profiler," *J. Med. Phys. Biophys.*, vol. 4, no. 1, pp. 95–102, 2017.

[28] D. Adhianto, C. Anam, H. Sutanto, and M. Ali, "Effect of Phantom Size and Tube Voltage on the Size-Conversion Factor for Patient Dose Estimation in Computed Tomography Examinations," *Iran. J. Med. Phys.*, vol. 17, no. 5, pp. 282–288, 2020.

[29] J. Zoetelief, H. W. Julius, and P. Christensen, "Recommendations for patient dosimetry in diagnostic radiology using thermoluminescence dosimetry," *Stand. Codes Pract. Med. Radiat. Dosim.*, p. 439, 2003.

[30] A. Jirasek and M. Hilts, "An overview of polymer gel dosimetry using x-ray CT," in *J. Phys.: Conf. Ser*, 2009, vol. 164, p. 12038.

[31] J. C. P. Heggie, J. K. Kay, and W. K. Lee, "Importance in optimization of multi-slice computed tomography scan protocols," *Australas. Radiol.*, vol. 50, no. 3, pp. 278–285, 2006, doi: 10.1111/j.1440-1673.2006.01579.x.

[32] F. Zarb, L. Rainford, and M. F. McEntee, "Image quality assessment tools for optimization of CT images," *Radiography*, vol. 16, no. 2, pp. 147–153, 2010.

[33] W. H. Moore, M. Bonvento, and R. Olivieri-Fitt, "Comparison of MDCT radiation dose: a phantom study," *Am. J. Roentgenol.*, vol. 187, no. 5, pp. W498–W502, 2006.

[34] M. K. Kalra *et al.*, "Strategies for CT radiation dose optimization," *Radiology*, vol. 230, no. 3, pp. 619–628, 2004.

[35] W. Huda, E. M. Scalzetti, and M. Roskopf, "Effective doses to patients undergoing thoracic computed tomography examinations," *Med. Phys.*, vol. 27, no. 5, pp. 838–844, 2000.

[36] D. P. Frush, "Review of radiation issues for computed tomography," in *Seminars in Ultrasound, CT and MRI*, 2004, vol. 25, no. 1, pp. 17–24.

[37] K. M. Kanal, B. K. Stewart, O. Kolokythas, and W. P. Shuman, "Impact of operator-selected image noise index and reconstruction slice thickness on patient radiation dose in 64-MDCT," *Am. J. Roentgenol.*, vol. 189, no. 1, pp. 219–225, 2007.

[38] M. Winkler and R. Mather, "CT Risk Minimized--By Optimal System Design," *DIAGNOSTIC IMAGING-SAN Fr.*, vol. 27, no. 7, p. 18, 2005.

[39] K. C. Lai and D. P. Frush, "Managing the radiation dose from pediatric CT," *Appl. Radiol.*, vol. 35, no. 4, p. A13, 2006.

[40] T. R. Goodman and J. A. Brink, "Adult CT: controlling dose and image quality," *Categ. course diagnostic Radiol. Phys. from Invis. to visible—the Sci. Pract. x-ray imaging Radiat. dose Optim. Chicago, Radiol. Soc. North Am.*, pp. 157–166, 2006.

Penumbra™

62

68

72

RED™

REPERFUSION CATHETERS

REDglide™ Technology
Designed to enhance delivery in tortuosity

62
.062" ID
1.93mm (0.76") OD
138cm Length

68
.068" ID
2.13mm (0.84") OD
132cm Length

72
.072" ID
2.16mm (0.85") OD
132cm Length